

# Femtosecond-Laser Direct Writing of Metallic Micro/Nanostructures: From Fabrication Strategies to Future Applications

Zhuo-Chen Ma, Yong-Lai Zhang,\* Bing Han, Qi-Dai Chen, and Hong-Bo Sun\*

The past decade has seen growing research interest in developing novel fabrication methodologies for metallic micro/nanostructures toward the rational design and integration of 0D to 3D metallic configurations. Among the various fabrication techniques, femtosecond-laser direct writing has emerged as a prominent approach to reach this goal and greatly facilitates the development of metallic micro/nanostructure-enabled applications. Here, a series of femtosecond-laser-mediated fabrication strategies, including the two-photon reduction of metal ions, template-assisted metal coating and metal filling, photodynamic assembly of metal nanoparticles, and selective nanoparticle sintering, are summarized. Additionally, abundant applications in microelectronics, metamaterials, near-field optics, microfluidics, micromechanics, and microsensors are introduced in detail. Current challenges and future perspectives in this field are also discussed.

## 1. Introduction


Recent years have witnessed rapidly increasing research interest in the micro/nanoscale structuring of metals. Owing to their unique optical and electronic properties, metallic micro/nanostructures are of great significance to a broad range of applications, such as metamaterials/metasurfaces,<sup>[1–5]</sup> electronics,<sup>[6,7]</sup> plasmonics,<sup>[8–13]</sup> surface enhanced Raman scattering (SERS),<sup>[14–18]</sup> and catalysis.<sup>[19–22]</sup> In the past decades, sustained research effort has been devoted to developing novel nanofabrication technologies that permit the rational design and precise control of metallic configurations from 0D to 3D. To date, several technologies, such as chemical synthesis,<sup>[23,24]</sup>

self-assembly,<sup>[25,26]</sup> optical/electron-beam lithography,<sup>[27,28]</sup> focused ion beam,<sup>[29,30]</sup> and 3D printing,<sup>[31,32]</sup> have demonstrated distinct advantages and revealed great potential for the flexible nanostructuring of metals. However, all of these technologies suffer from insuperable problems in fabricating arbitrary 3D metallic micro/nanostructures. For instance, chemical routes are versatile and powerful for preparing metallic nanostructures ranging from 0D nanoparticles to 3D features,<sup>[23,24]</sup> but metallic micro/nanostructures with complex configurations cannot be synthesized directly. Self-assembly approaches provide a controllable avenue to construct 2D and 3D micro/nanostructures by making full use of the interactions between individual nano-building-blocks,<sup>[25,26]</sup> but the assembly process cannot be pre-designed freely. To construct metallic structures according to design, lithography techniques have been widely adopted for fabricating 2D metal patterns,<sup>[27,28]</sup> and the resolution can currently reach a few nanometers; nevertheless, lithography strategies are naturally 2D processing routes and are not capable of 3D fabrication. Recently, 3D-printing technology has made it possible to construct 3D metallic structures on a macroscopic scale.<sup>[31,32]</sup> However, it is difficult to improve the resolution to the microscale level, not to mention the nanoscale. Currently, the designable fabrication and integration of complex 3D metallic micro/nanostructures for the development of metallic micro/nanodevices remains a challenge.

As a powerful 3D micro/nanofabrication technique, femtosecond-laser direct writing (FsLDW) has emerged as a nano-enabler for the designable fabrication of micro/nanostructures based on a wide range of materials.<sup>[33–42]</sup> Especially for metals, FsLDW technology is distinguished by its mask-free processing capability, arbitrary shape designability, high spatial resolution, ease of integration, and suitability for various nonplanar substrates. In the past decade, with the help of FsLDW technology, great success has been achieved in the fabrication and integration of metallic micro/nanostructures, promoting the rapid development of a series of scientific fields. Here, we summarize the recent advances of this powerful technology in the fabrication of metallic micro/nanostructures and highlight its contributions to metallic micro/nanostructure-enabled functional devices. The general concept of FsLDW strategies and future applications is illustrated in **Figure 1**. First, several

Dr. Z.-C. Ma, Prof. Y.-L. Zhang, B. Han, Prof. Q.-D. Chen  
State Key Laboratory of Integrated Optoelectronics  
College of Electronic Science and Engineering  
Jilin University  
2699 Qianjin Street, Changchun 130012, China  
E-mail: yonglaizhang@jlu.edu.cn

Prof. H.-B. Sun  
State Key Lab of Precision Measurement Technology and Instruments  
Department of Precision Instrument  
Tsinghua University  
Haidian, Beijing 100084, China  
E-mail: hbsun@tsinghua.edu.cn

 The ORCID identification number(s) for the author(s) of this article can be found under <https://doi.org/10.1002/smt.201700413>.

DOI: 10.1002/smt.201700413

femtosecond-laser fabrication strategies that enable the designable structuring of metals, including the two-photon reduction of metal ions, template-assisted metal coating or filling, photo-dynamic assembly of metal nanoparticles, and laser selective nanoparticle sintering, are summarized and discussed. For an overview of the diverse fabrication strategies based on the FsLDW of metallic micro/nanostructures, typical studies are summarized in Table 1. Then, we review the broad applications of functional metallic structures fabricated by FsLDW, including microelectronics, metamaterials, near-field optics, microfluidics, micromechanics, and microsensors (the upper part of Figure 1). As an overview of the broad applications based on the FsLDW of metallic micro/nanostructures, typical studies in various fields are summarized in Table 2. Finally, the current challenges and future perspectives in this field are discussed.

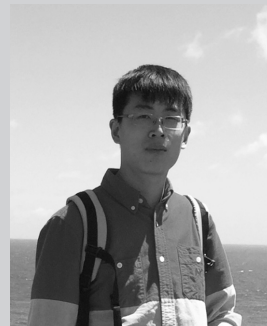
## 2. Photochemical/Photophysical Strategies

### 2.1. TPA-Induced Photoreduction of Metal Ions

Through a two-photon absorption (TPA) process,<sup>[43–45]</sup> metal ions can be reduced into neutral atoms; thus, femtosecond-laser two-photon fabrication naturally holds promise for fabricating metallic 3D micro/nanostructures by a process similar to two-photon polymerization (TPP).<sup>[46–49]</sup> In a typical TPA process, two photons are absorbed simultaneously to gain enough photon energy and excite molecules to a high energy state. The frequencies of the absorbed photons can be either similar or different. In addition, the sum of the photon energy should be equal to the energy difference between the two energy levels.<sup>[43–45,50]</sup> TPA is a third-order nonlinear optical effect, which relies largely on the square of the laser intensity.<sup>[51,52]</sup> Unlike linear optical absorption, which can be easily realized at relatively lower laser intensities, to achieve TPA, a laser with high intensity should be employed. Focused femtosecond-laser pulses with a typical peak intensity as high as  $10^{14}$ – $10^{15}$  W m<sup>-2</sup> enable the confinement of a large number of photons within an extremely small focus region. Because of the threshold effect of the TPA process, photoinduced reactions only occur at the central region of the focal point, and, thus, a much higher spatial resolution that goes beyond the diffraction limit can be realized.<sup>[42,53–57]</sup> There are also some constraints for TPA fabrication, for instance: (i) two-photon sensitizers are usually needed to enable a high-efficiency absorption process, (ii) the materials should be transparent at the excitation laser wavelength to ensure transmission of the incident laser, and (iii) transparent substrates are usually adopted.

A typical setup for TPA fabrication consists of four parts: a laser source and light-direction system, a beam-focusing and motion-stage system, a computer-aided control system, and a charge-coupled-device-based monitoring system.<sup>[41]</sup> The femtosecond laser is tightly focused on the materials located on the motion stage by using an objective lens with high numerical apertures, and the computer-aided control system can program the laser scanning routes, guiding the entire fabrication.

To date, FsLDW technology has been widely employed for fabricating metallic micro/nanostructures based on silver,



in MEMS, near-field optics, and integrated microfluidic chips.

**Zhuo-Chen Ma** received his Ph.D. degree in 2016 from the College of Electronic Science and Engineering, Jilin University. He is currently a postdoctoral researcher at the College of Physics, Jilin University. His research work is mainly focused on laser fabrication of metallic micro/nanostructures and their applications



awarded a “Hong Kong Scholar” postdoctoral fellowship and worked at the Center of Super Diamond and Advanced films (COSDAF), City University of Hong Kong. His research interests include laser micro/nanofabrication of functional micro/nanostructures, smart actuators, and Bio-MEMS.

**Yong-Lai Zhang** received his B.S. degree in 2004 and Ph.D. degree in 2009 from Jilin University, China. In 2010, he joined the faculty in the State Key Laboratory on Integrated Optoelectronics, College of Electronic Science and Engineering, Jilin University. In 2011, he worked as a research professor in Yonsei University, Korea. After that, he was



at Jilin University, and in 2017 he moved to Tsinghua University, China. His research focuses on laser micro/nanofabrication and ultrafast spectroscopy.

**Hong-Bo Sun** received his Ph.D. degree in 1996 from Jilin University, China. He worked as a postdoctoral researcher at the University of Tokushima, Japan, from 1996 to 2000, and then as an assistant professor in Department of Applied Physics, Osaka University from 2000 to 2006. From 2006, he worked as a Changjiang-Scholar professor

gold, palladium, and platinum through a two-photon reduction process (shown in Table 1), and several photochemical/photophysical strategies based on the TPA process have been successfully proposed, including the TPA-induced photoreduction of metal ions from solution, the TPA-induced photoreduction of metal ions in matrixes, and the TPA-induced simultaneous photopolymerization and photoreduction of metal ions

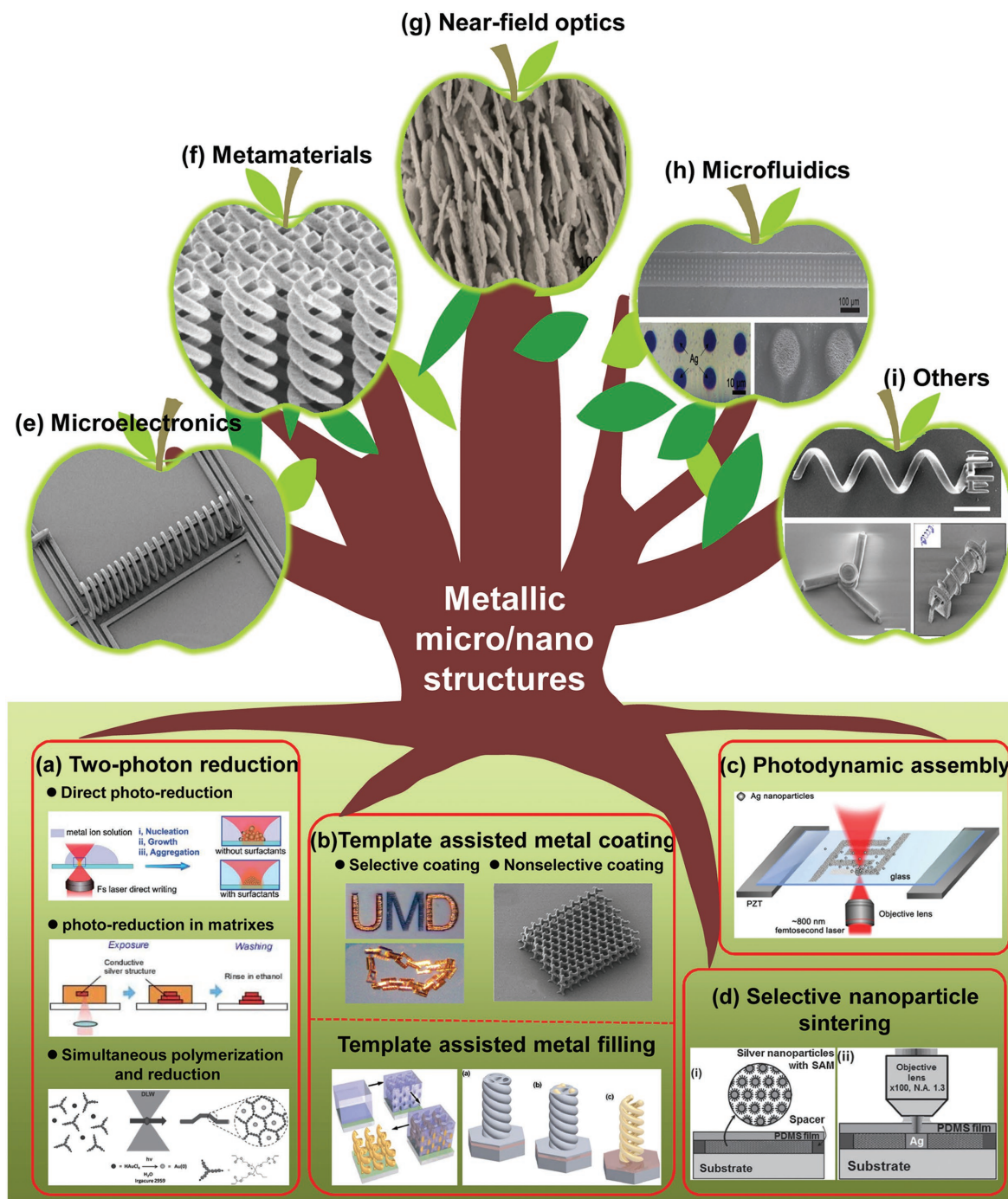


**Figure 1.** General concept of FsLDW strategies of metallic micro/nanostructures and their related broad application fields. a–d) Methods of two-photon reduction of metal ions (a), template-assisted metal coating or filling (b), photodynamic assembly (c), and selective nanoparticle sintering (d). e–i) Applications in microelectronics (e), metamaterials (f), near-field optics (g), microfluidics (h), and other fields, such as micromechanics (i). a) Top image: reproduced with permission.<sup>[41]</sup> Copyright 2010, Elsevier; middle image: reproduced with permission.<sup>[74]</sup> Copyright 2008, Optical Society of America; bottom image: reproduced with permission.<sup>[62]</sup> Copyright 2016, Wiley-VCH. b) For selective coating: upper image: reproduced with permission.<sup>[50]</sup> Copyright 2007, Wiley-VCH; lower image: reproduced with permission.<sup>[106]</sup> Copyright 2006, American Chemical Society. For nonselective coating: image: reproduced with permission.<sup>[87]</sup> Copyright 2013, The Royal Society of Chemistry. For template-assisted metal filling: left image: reproduced with permission.<sup>[109]</sup> Copyright 2009, American Association for the Advancement of Science; right image: reproduced with permission.<sup>[111]</sup> Copyright 2015, Optical Society of America. c) Image: reproduced with permission.<sup>[123]</sup> Copyright 2015, Institute of Physics. d) Image: reproduced with permission.<sup>[127]</sup> Copyright 2011, Wiley-VCH. e) Reproduced with permission.<sup>[50]</sup> Copyright 2007, Wiley-VCH. f) Reproduced with permission.<sup>[111]</sup> Copyright 2015, Optical Society of America. g) Reproduced with permission.<sup>[135]</sup> Copyright 2011, The Royal Society of Chemistry. h) Reproduced with permission.<sup>[19]</sup> Copyright 2012, The Royal Society of Chemistry. i) Upper image: reproduced with permission.<sup>[86]</sup> Copyright 2012, The Japan Society of Applied Physics; lower images: reproduced with permission.<sup>[93]</sup> Copyright 2012, Wiley-VCH.

**Table 1.** Diverse fabrication strategies involving the FsLDW of metallic micro/nanostructures.

Strategy	Mechanism	Precursor	Type of metal	Resolution	Resistivity	Advantages	Disadvantages	Ref.
Two-photon reduction	Direct photoreduction from solution	Metal-ion aqueous solution	Silver, gold, palladium, platinum	≈120 nm	$5.30 \times 10^{-8} \Omega \text{ m}$	1. Single step for the direct fabrication of metallic structures; 2. Especially high utility for 2D features	1. Rough surface; 2. Poor mechanical strength	[59–61,65–69]
	Photoreduction in a matrix	Metal-ion-fused matrix	Silver, gold	sub-100 nm	$3.48 \times 10^{-7} \Omega \text{ m}$		1. Relatively poor conductivity; 2. High dependence on the matrix or photoresist	[58,70–79]
	Simultaneous photopolymerization and photoreduction	Metal-ion-doped photoresist	Gold	150 nm	$9.60 \times 10^{-8} \Omega \text{ m}$			[62–64]
Metal deposition utilizing a prefabricated template	Nonselective/selective metal coating	Prefabricated template surface	Nickel, titanium, tungsten, molybdenum, silver, copper, gold	sub-100 nm	$8.20 \times 10^{-8} \Omega \text{ m}$	1. Metallodielectric microstructures of almost arbitrary geometries and metals	1. Inability to obtain highly homogeneous metal coating	[50,80–88,91,93–108]
	Metal filling	Prefabricated void template	Gold, copper, nickel	sub-300 nm	–	1. 3D solid metal structures; 2. High mechanical strength; 3. Almost any metal	1. Inability to create complex shapes, such as wood-pile configuration	[109–115]
Photodynamic assembly	Optical trapping	Metal-nanoparticle ink	Silver, gold	190 nm	$5.50 \times 10^{-8} \Omega \text{ m}$	1. Single step for assembly into metallic structures; 2. Particularly high utility for 2D geometries	1. Inability to create 3D structures	[123,124]
Selective nanoparticle sintering	Thermal melting	Metal-nanoparticle thin film	Silver, copper	380 nm	$1.80 \times 10^{-7} \Omega \text{ m}$			[127,128]

(depicted in Figure 1a). Generally, in the TPA-induced photoreduction of metal ions, appropriate reductants, such as polyvinylcarbazole, coumarin or trisodium citrate for silver ions;<sup>[58–60]</sup> glycinate ionic liquid or Irgacure 2959 for gold ions;<sup>[61,62]</sup> and iron (III) oxalate for palladium and platinum ions,<sup>[20]</sup> are commonly used. In addition, the use of photosensitizers is also necessary to suppress the thermal effect by decreasing the threshold laser power. Typical photosensitizers that are frequently adopted in the TPA fabrication of metallic structures include coumarin,<sup>[59]</sup> AF380,<sup>[63,64]</sup> and bis-electron-acceptor-substituted p-conjugated organic chromophores.<sup>[58]</sup>

### 2.1.1. Direct Photoreduction of Metal Ions from Solution

Kawata and co-workers first reported the TPA-induced photoreduction of metal ions for fabricating metallic micro/nanostructures.<sup>[65]</sup> In their work, aqueous solutions of silver nitrate and tetrachloroauric acid were prepared for the fabrication of silver and gold microstructures, respectively. Metal ions can be directly reduced by a tightly focused femtosecond pulsed laser via a TPA process. A self-standing metallic microstructure with a low electrical resistivity, only 3.3 times larger than that of bulk

silver, was demonstrated. Later, the photoreduction of silver ions in aqueous solution was further improved with the help of the two photon-sensitive dye coumarin 440.<sup>[59]</sup> Excitation of the dye through a TPA process enabled the reduction of silver ions under relatively low laser intensity. In this way, the localized thermal effect is significantly suppressed, and much finer silver microstructures with subdiffraction-limit resolution could be successfully fabricated. As a typical example, a conductive silver nanowire with a minimum width of 400 nm was obtained.

Although the TPA photoreduction of metal ions enables the fabrication of metallic microstructures, obtaining fine structures that are comparable to photopolymers is quite difficult. During the formation of a metal structure, ion diffusion and particles aggregation are unavoidable, resulting in a very rough metal surface and distorted configuration. To solve this problem, Duan and co-workers developed a surfactant-assisted TPA approach using fatty salts with different carbon chain lengths to control the photoreduction (Figure 2a).<sup>[66,67]</sup> In this way, the feature size of the resultant silver structures was significantly reduced. Moreover, the surface smoothness was improved by increasing the chain length of the fatty salts. With the help of surfactant molecules, the diameters of the as-formed silver nanoparticles could be reduced to tens

**Table 2.** Broad applications of the FSLDW of metallic micro/nanostructures.

Application area	Device/structure	Fabrication method	Specified usage	Ref.
Microelectronics	Microinductor	Selective metal coating onto a prefabricated template	Integrated circuits	[106]
	Metal nanowiring on nonplanar substrates	Two-photon reduction	3D electrical interconnection	[60]
	Metal microelectrodes	Photodynamic assembly	Microelectrodes in certain working devices, such as organic FETs (OFETs)	[124,127,129]
Metamaterials	2D silver rod pair array	Two-photon reduction	Negative permeability	[130]
	2D arrays of U-shaped gold split-ring resonators	Two-photon reduction	Negative permittivity	[68]
	3D magnetic metamaterial	Metal coating onto a prefabricated template	Magnetic resonance with $\text{Re}(\mu) < 0$	[2]
	3D standing U-shaped metamaterial	Metal coating onto a prefabricated template	Control or detection of the polarization of light	[97]
	3D gold helix metamaterial	Metal electrodeposition into a prefabricated template	Circular polarizer	[109]
Near-field optics	Hierarchical silver nanoplate	Two-photon reduction	High SERS enhancement factor (EF) of $\approx 10^8$	[135]
	3D gold nanostructure	Two-photon reduction	Successful SERS detection of fungicide thiabendazole	[136]
Microfluidics	SERS monitors in microfluidic channels	Two-photon reduction	Real-time detection of on-chip chemical reactions	[135]
	Silver-microflower arrays	Two-photon reduction	Robust catalytic sites for the reduction of 4-NP to 4-aminophenol (4-AP)	[19]
	Catalytic Pd and Pt microstructures within a 3D microfluidic environment	Two-photon reduction	Site-specific catalysis in microfluidic systems toward flow generation, fluid mixing, propulsion, collection, and transport	[20]
Micromechanics	Microrotor, microscrew	Metal coating onto a prefabricated template	Movable metallic microparts in MEMS or LoC systems	[86]
	Magnetic microstirrer	Metal coating onto a prefabricated template	Smart micromachines with remote control capability	[85]
	Magnetic helical micromachines	Metal coating onto a prefabricated template	Micromanipulation of biological cells or drug delivery in vivo	[93]
Microsensors	Palladium nanostructure	Two-photon reduction	Hydrogen sensor	[69]

of nanometers. Thus a silver line with nanometer-scale resolution,  $\approx 120$  nm in width, was successfully achieved for the first time. Furthermore, Duan and co-workers also succeeded in fabricating 3D freestanding silver microstructures, such as pyramids. However, the presence of surfactants also has negative effects. The electrical conductivity of the resultant metallic structures is poor, which limits their applications in electronics. To improve the conductivity, Xu et al. employed trisodium citrate as a reducing agent to prepare a silver precursor for TPA photoreduction (Figure 2b).<sup>[60]</sup> Silver nanowires with a low resistivity of  $\approx 1.7 \times 10^{-7} \Omega \text{ m}$ , only ten times higher than that of bulk silver ( $1.6 \times 10^{-8} \Omega \text{ m}$ ), were successfully achieved. The inset of Figure 2b shows the TPA-induced photochemical reaction, in which silver ions in the form of  $\text{Ag}(\text{NH}_3)_2^+$  are reduced to neutral silver atoms, forming silver nanoclusters along the laser scanning path. At the same time, trisodium citrate used as the reducing agent was transformed to acetone-1,3-dicarboxylate. Here, citrate also acts as an inhibitor of silver nanoparticle growth, which helps form a smooth surface.

In addition to silver micro/nanostructures, femtosecond-laser TPA photoreduction strategies have also been applied to other metals.<sup>[20,61,68,69]</sup> Duan and co-workers proposed a facile ionic liquid-assisted femtosecond-laser TPA photoreduction approach to fabricate subwavelength gold nanostructures in a  $\text{AuCl}_4^-$  ion aqueous solution.<sup>[61,68]</sup> With the use of a suitable ionic liquid and optimized laser fabrication parameters, the resolution of the gold nanostructure could reach as low as 228 nm, far beyond the optical diffraction limit. More importantly, the conductivity of the as-fabricated gold nanostructure was on approximately the same order as that of bulk gold. In addition, Kaehr and co-workers reported a straightforward TPA process to fabricate microscale patterns of nanocrystalline palladium and platinum by employing  $(\text{NH}_4)_2[\text{PtCl}_4]$  or  $(\text{NH}_4)_2[\text{PdCl}_4]$  as metal salts and  $(\text{NH}_4)_3[\text{Fe}(\text{C}_2\text{O}_4)_3]$  as a reducing agent.<sup>[20]</sup> These two metals displayed unique advantages in catalytic and electrochemical properties over silver and gold.

Although rapid progress has been made in recent years, several serious problems still restrict the broad application of

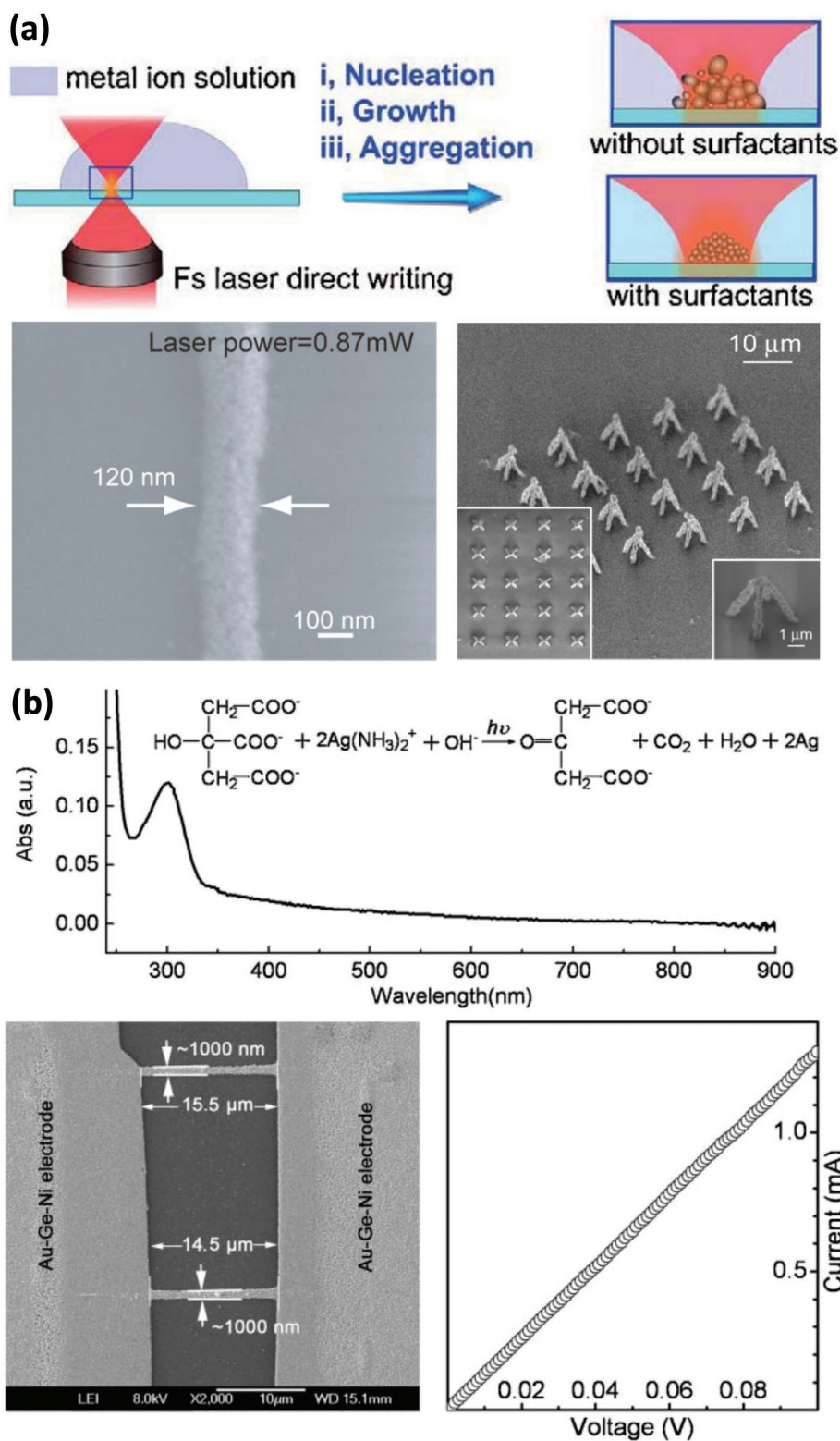


**Figure 2.** Representation of the direct two-photon reduction of metal ions from solution. a) Schematic illustration of the fabrication of metallic features by the photoreduction of metal ions. Surfactants were adopted as growth inhibitors of the metal particles, thus facilitating a high resolution of  $\approx 120$  nm and the fabrication of 3D freestanding nanostructures, such as pyramids. Reproduced with permission.<sup>[67]</sup> Copyright 2009, Wiley-VCH. b) Scheme for the femtosecond laser two-photon reduction of silver ions using trisodium citrate as a reducing agent. The absorption spectrum demonstrated that the photoreduction was a TPA process (upper). The resistivity of the fabricated silver nanowire was measured by patterning it between two electrodes (lower). Reproduced with permission.<sup>[60]</sup> Copyright 2010, Wiley-VCH.

the TPA fabrication of metallic micro/nanostructures. First, the TPA-induced photoreduction reaction at the focal region consumes most of the metal ions, and supplementation of the metal source based on ion diffusion is generally insufficient. The lack of sufficient metal ions results in a rough surface and even a discontinuous structure. Moreover, the as-formed metal structures exert additional influence on the subsequent processing. For instance, when the incident laser irradiates the metal structures, the thermal effect and localized surface plasma resonance (LSPR) will undoubtedly affect the aggregation and crystallization of metal nanoparticles, but these processes are wholly uncontrollable. These problems constitute the main barrier to fabricating 3D metal structures with fine morphology and robust mechanical strength.

### 2.1.2. Photoreduction of Metal Ions in Matrixes

Owing to the abovementioned limitations, the fabrication of fine 3D metallic structures directly from a metal-ion solution remains challenging. Therefore, researchers have explored an alternative method to make metal micro/nanostructures. A transparent matrix doped with metal ions was used for femtosecond-laser photoreduction. The matrix cannot only support the as-fabricated metallic structures but also serves as a reducing agent in special cases, promoting the reduction of metal ions. In this way, various metallic 3D micro/nanostructures have been successfully fabricated through a TPA process.

A pioneering study reported by Dunn and co-workers in 2000 gave a typical example, in which a porous silicate sol-gel matrix loaded with  $\text{AgNO}_3$  was used for femtosecond-laser fabrication.<sup>[70]</sup> To form a latent image, predesigned structures were written into the interior of the matrix. Next, the further development of silver patterns via the controlled reduction of  $\text{AgClO}_4$  solution led to the formation of the final silver structures. Unfortunately, however, the as-obtained silver microstructures showed very low electrical conductivity and poor mechanical strength, since they consisted mainly of discrete nanoparticles. Later, in 2002, Stellacci et al. demonstrated the fabrication of a 3D log-pile-type structure of silver lines in a polyvinylcarbazole matrix containing the silver salt  $\text{AgBF}_4$ , alkanethiol-coated silver nanoparticles as seeds, and a photoreducing dye as a sensitizer.<sup>[58]</sup> The resistivity of the resultant silver lines was measured to be  $10^{-3} \Omega \text{ m}$ , approximately three orders of magnitude larger than that of bulk silver. Using composites analogous to that used for silver, they also successfully fabricated copper and gold microstructures, revealing the versatility of this method for the designable fabrication of 3D metallic structures. However, obvious deformation was observed after the removal of the polymer matrix. In addition to laser direct writing, laser holography was also employed to produce metallic gratings. In 2003, Kaneko et al. reported the fabrication of a 2D gold-nanoparticle grating by the two-beam laser interference treatment of a polymer film infused with  $\text{HAuCl}_4$ .<sup>[71]</sup> As in previous studies, the as-prepared gold patterns were not continuous, resulting in poor conductivity. Then, in 2005, Fourkas and co-workers presented a method for making 2D silver patterns using a poly(vinylpyrrolidone) (PVP) film containing silver nitrate as a matrix.<sup>[72]</sup> After the formation of the silver

structure, the polymer could be washed away to leave silver patterns consisting of large numbers of silver nanoparticles on the substrates. However, the deposited metallic features were not electrically conductive at all. To solve this problem, Fourkas and co-workers subsequently attempted the electroless deposition of copper on the silver structures.<sup>[73]</sup> The conductivity of the metallic features was thereby greatly improved. Moreover, they further demonstrated the fabrication of metallic features on 3D polymeric structures fabricated by TPP, enabling the integration of electrical or optical components into 3D polymeric microstructures. In these studies, further electroless plating was necessary to obtain conductive structures. To achieve better conductivity, Maruo et al. successfully created continuous 2D and 3D silver structures by increasing the density of silver nitrate loaded in the PVP film.<sup>[74]</sup> The resistivity of the fabricated silver features could reach  $3.48 \times 10^{-7} \Omega \text{ m}$ , only  $\approx 22$  times higher than that of bulk silver. Considering the poor stability of silver in the atmosphere, gold is generally considered a better choice for conductive metallic structures. Therefore, Vurth et al. introduced the two-photon photoreduction of gold in a polystyrene sulfonate matrix infused with  $\text{HAuCl}_4$  as a metal source and a ruthenium dye as a photoinitiator.<sup>[75]</sup> In their study, an additional electroless plating process was also necessary to make the gold structures conductive.

In addition to the fabrication of continuous metallic structures, this technique enables the fabrication of suspended and discrete structures by the space-selective deposition of metals in a matrix, providing an opportunity to make discontinuous metallic structures beyond general interconnected features.<sup>[76–79]</sup> This ability could be considered a unique advantage over other methods. For instance, the fabrication of 3D arrays composed of fully disconnected metal microstructures enables the creation of bulk optical or infrared metamaterials comprising coupled metal units. However, for general 3D fabrication crafts, this goal is highly challenging. Using the matrixes as a supporting skeleton makes the fabrication of 3D-disconnected metallic microstructures much easier. Ameloot et al. used a highly porous and photocatalytically active metal-organic framework (MOF) as a single-crystal matrix and demonstrated the patterning of a set of two identical 2D codes written inside the MOF crystal (**Figure 3**).<sup>[76]</sup> Figure 3a shows a schematic of the direct laser writing of silver patterns inside an MOF crystal immersed in silver nitrate solution. Figure 3b shows the top and side views of the two codes written in the MOF crystal placed  $10 \mu\text{m}$  apart in the vertical direction. This kind of fabrication strategy may enable the production of metallo-dielectric structures that might be useful for 3D discrete optical or electrical devices. In 2012, Mazur and co-workers demonstrated the writing of disconnected 3D silver structures with a 300 nm resolution in a PVP matrix.<sup>[77]</sup> However, the silver patterns had a short shelf life, and the resolution was not high enough for optical-metamaterial applications. This obstacle was overcome later in 2015. Gelatin was selected as an alternative matrix because it possesses several distinct advantages over other materials; for instance, it is an inexpensive, nontoxic, biodegradable, and water-soluble polymer that has gelling properties similar to those of hydrogels, thus enabling the fabrication of thicker and more durable structures.<sup>[78]</sup> The authors successfully patterned sub-100 nm silver features and

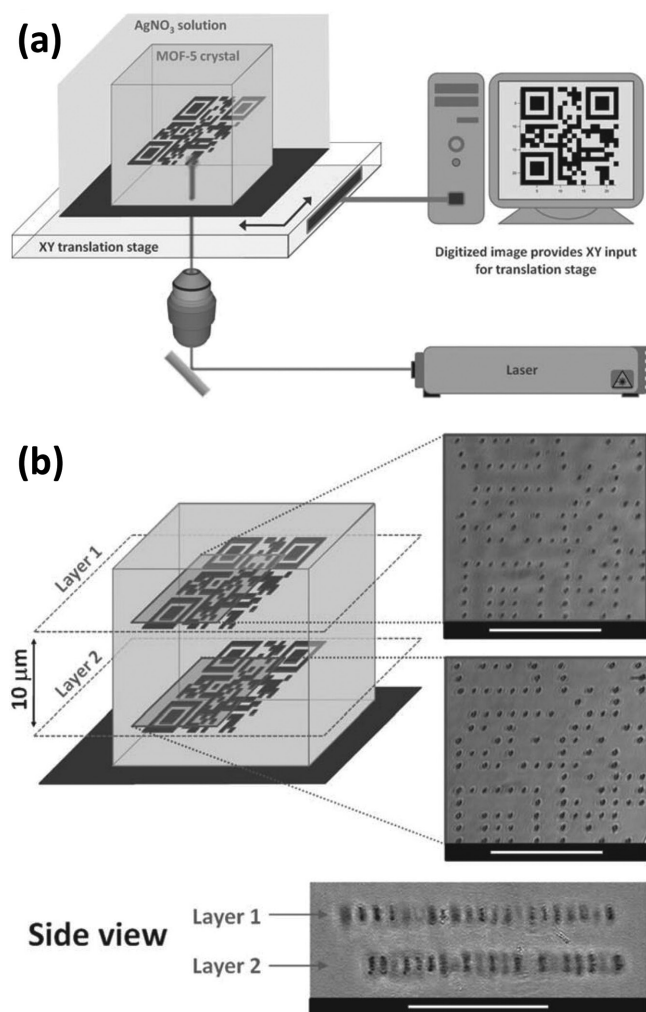


**Figure 3.** Fabrication of metallic nanostructures by the photoreduction of metal ions inside an MOF matrix. a) Schematic illustration of the direct laser writing of silver patterns in an MOF-5 crystal immersed in silver nitrate aqueous solution. b) 3D discrete patterns of two layers written in the MOF-5 matrix with a separation of  $10\ \mu\text{m}$  in the vertical direction. The upper and lower SEM images are the top view and side view, respectively. Scale bar:  $25\ \mu\text{m}$ . Reproduced with permission.<sup>[76]</sup> Copyright 2011, Wiley-VCH.

produced more than 16 layers of disconnected metallic structures. In addition, gelatin was experimentally verified to have transparency windows that satisfied the demand for potential applications in the optical and terahertz spectral regions.

The use of matrixes has revealed a series of positive effects for the designable fabrication of metallic micro/nanostructures. For instance, the as-formed structures can be well supported, which enables the fabrication of suspended and discontinuous structures. However, at the same time, the matrix also introduces new problems, among which the poor conductivity is serious. The presence of isolated matrix networks inevitably influences the conductivity of the metal structures, making them unsuitable for electronic applications. The poor conductivity lies in the discontinuous metal structures in the polymer matrix, since only a limited amount of metal ions, mainly in the range of  $\approx 0.1$  to  $1\ \text{M}$ , can be loaded into the matrix material.<sup>[72–79]</sup>

Such limitation can be attributed to the presence of polymer matrix and the solubility of metal ions. Nevertheless, metallic structures fabricated using this technique are promising for optical applications, such as 3D photonic devices and metamaterials, as the metal is optically dense, and the structures fabricated in this way are usually much smaller than the wavelength of visible light.

### 2.1.3. Simultaneous Photopolymerization and Photoreduction of Metal Ions

In addition to the abovementioned strategies, the simultaneous photopolymerization and photoreduction of metal ions in a single direct-writing procedure is also capable of fabricating 3D metallic structures.<sup>[62–64]</sup> Generally, if metal ions can be homogeneously doped into a photoresist, subsequent laser treatment will not only trigger the photopolymerization of the polymer but also lead to the simultaneous photoreduction of metal ions, thereby enabling the 3D fabrication of metallic structures in a similar manner to TPP.

As a typical example, Prasad and co-workers first demonstrated the two-photon fabrication of subdiffraction-limited gold nanostructures in a photoresist film using a precursor containing a two-photon dye (AF380),  $\text{HAuCl}_4$ , and an SU-8 photoresist, enabling the production of gold nanoparticle-doped polymeric lines as narrow as  $150\ \text{nm}$ .<sup>[64]</sup> In their work, in situ gold-ion reduction and the cationic polymerization of SU-8 were simultaneously accomplished. The patterned gold lines showed relatively low resistivity, only four times higher than that of bulk gold, due to the high loading fraction of the gold precursor and the formation of relatively small, densely packed gold nanoparticles inside the photoresist.<sup>[63]</sup> However, their work mainly focused on the fabrication of 2D conductive patterns, and the development of 3D metallic conductive microstructures remained challenging at the time. Subsequently, in pursuit of 3D metallic conductive microstructures, Wegener and co-workers reported the synthesis of a novel water-soluble photoresist that was suitable for metal doping and demonstrated the patterning of 3D metallic structures by simultaneous photopolymerization and photoreduction (Figure 4).<sup>[62]</sup> As shown in Figure 4a, the photoresist composite consisted of an acrylate-functionalized poly(ethylene glycol) derivative (PEG-triacry),  $\text{HAuCl}_4$ , and Irgacure 2959 as the photoinitiator. To further improve the conductivity of the resultant structures, a thermal-annealing process was implemented. In this way, the conductivity of the gold lines was increased to  $2.2 \times 10^6\ \text{S m}^{-1}$ , which was only 20 times lower than that of bulk gold ( $4.1 \times 10^7\ \text{S m}^{-1}$ ). The composite photoresist was also employed for the fabrication of truly 3D connections between separated gold pads (Figure 4b,c), revealing great potential in 3D electronics.

The strategy of simultaneous photopolymerization and photoreduction is superior to conventional routes because the metal nanoparticles formed during laser processing can be immediately immobilized within the polymer matrix, which can effectively suppress the diffusion and aggregation of the nanoparticles, leading to a finer structure and much higher resolution. Accordingly, this technique has been commonly



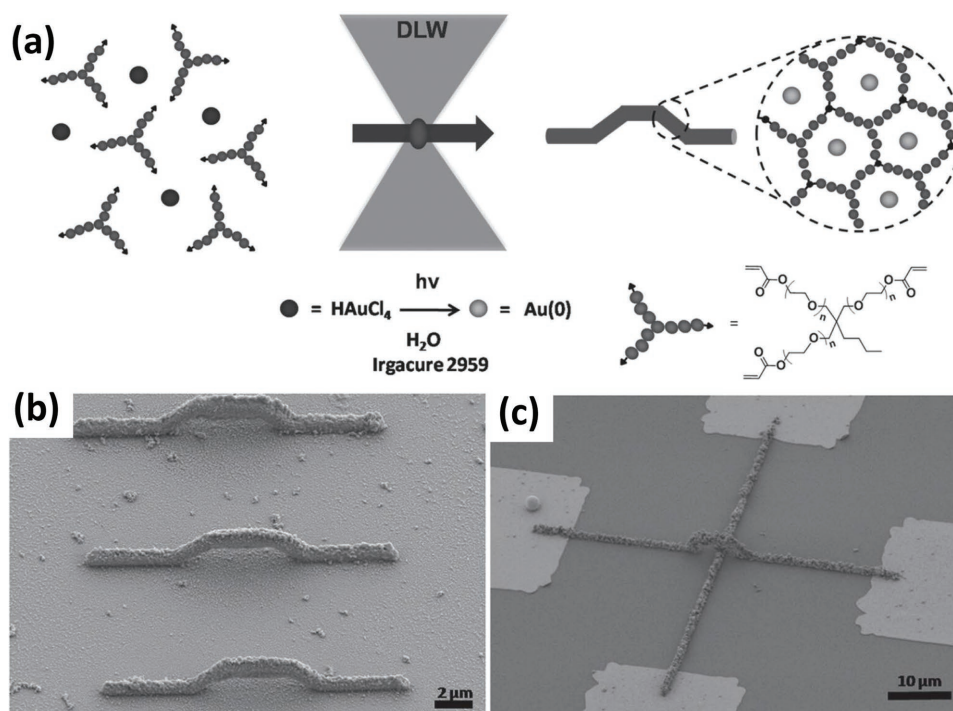


**Figure 4.** a) Schematic demonstration of the fabrication process for the simultaneous photopolymerization and photoreduction of HAuCl<sub>4</sub> via TPA. b) SEM image of 3D microarches fabricated by the laser direct writing of a gold precursor-doped photoresist. c) SEM image of true 3D metallic connections between the gold pads obtained by fabricating two metallic wires perpendicularly. Reproduced with permission.<sup>[62]</sup> Copyright 2016, Wiley-VCH.

recognized as a promising approach to prepare truly 3D free-standing metallic microstructures with both high resolution and high conductivity. However, to achieve further improvements, some issues should be considered. For instance, how can the doping contents of metal be increased? Is it possible to remove the polymers and maintain the metallic structures? In the case of metal-ion-doped photoresists, the limited metal content is also an issue. According to the reported results, the loaded content of metal is generally in the range of 10–50% by weight.<sup>[62–64]</sup> Factors that limit the loading contents include the solubility of metal ions in the photoresist and the negative impacts from the as-formed metal structures, such as the thermal effect, LSPR, and the crystallization effect. Therefore, it is necessary to balance the loading contents of metals and the morphology quality of the resultant structures.

## 2.2. Template-Assisted Metal Coating and Metal Filling

To address the difficulties in directly fabricating truly 3D metallic structures by the TPA-induced photoreduction of metal ions, an alternative method using prefabricated 3D structures as templates has emerged as a solution, with examples including template-assisted surface metal coating and metal filling into template structures. In these approaches, various polymeric 3D structures are fabricated beforehand by TPP as functional templates. Then, metal plating technologies, e.g., electroless plating, chemical vapor deposition, and physical vapor deposition, are employed for the metallization of the template surface, or metal-filling techniques such as electroplating

are used for filling into the void template, thereby enabling the fabrication of metallic microstructures with arbitrary 2D or 3D shapes. In this section, we summarize the studies on this approach and classify them into two categories: metal coating and metal filling (depicted in Figure 1b).

### 2.2.1. Nonselective/Selective Metal Coating

The metallization of polymeric structures fabricated via TPP has been proven to be an effective approach to fabricate 3D metal structures. By controlling the experimental conditions, a wide variety of metallization reactions have been conducted successfully on the surface of different polymers. As a typical route, electroless plating has been widely employed for metal coating.<sup>[80–87]</sup> For instance, Misawa and co-workers first reported the coating of nickel on SU-8 microstructures fabricated by TPP.<sup>[80]</sup> Kaneko et al. coated a silver layer on an SCR 500 template.<sup>[81]</sup> Duan and co-workers reported the electroless plating of a Ni–P alloy layer on a polymer surface created by TPP.<sup>[85]</sup> The hardness and modulus of the Ni–P/polymer composite film were improved to 1.74 and 34.93 GPa, respectively, corresponding to a tenfold and ninefold enhancement of the polymer film. The electroless plating technique has been widely used owing to the low cost; applicability to a variety of metals, such as nickel, silver and copper; and ease of operation without the need of vacuum conditions.<sup>[80,83,88–90]</sup> The metal thickness can be well controlled by tuning the reaction time normally with a deposition rate of  $\approx 1\text{--}10 \text{ nm s}^{-1}$ . Nevertheless, the surface roughness of the metal coatings prepared in this way is

relatively high. In addition, other problems with respect to the use of complicated and toxic chemicals in the plating solution, as well as the gradually changed reagent concentration during electroless plating also restrict the broad application of this technique in the fabrication of metallic micro/nanostructures.

As alternatives, other surface-coating techniques, such as chemical vapor deposition (CVD),<sup>[2,91]</sup> atomic-layer deposition (ALD),<sup>[92]</sup> and physical vapor deposition (PVD) techniques, including electron-beam evaporation<sup>[93–96]</sup> and sputtering,<sup>[97–100]</sup> have also been used for metal coating. The CVD technique, which utilizes gas-phase metal sources, enables controllable metal coating.<sup>[2,91]</sup> The film thickness can reach tens of nanometers with a deposition rate of  $\approx 1\text{--}10\text{ nm s}^{-1}$ . Compared with electroless plating, the surface roughness of the resultant metal films prepared by CVD is significantly improved. However, CVD requires the specific metal source, gas chambers and temperature-control systems. Currently, the types of metals that can be deposited on polymeric micro/nanostructures are still limited and mainly include tungsten and molybdenum (Table 1). Moreover, because CVD coating is usually carried out at high temperature, precoating of the polymer structures with protective materials with high thermal stability is necessary, which further complicates the process. To achieve a much thinner thickness of the metal coating layer, the ALD technique can be applied to the polymer structures.<sup>[92]</sup> Compared with the aforementioned techniques, the metal coating deposited by ALD is very uniform and smooth, and the deposition rate can be controlled to as low as  $0.1\text{ nm s}^{-1}$ . However, the ALD equipment is expensive, and the applicable metals are quite limited. PVD techniques, such as thermal/electron-beam evaporation and sputtering deposition, are applicable to many kinds of metals including nickel, silver, and gold.<sup>[93–100]</sup> The film thicknesses can be tuned from tens to hundreds of nanometers with deposition rates in the range of  $0.1\text{--}10\text{ nm s}^{-1}$ . However, thermal/electron-beam evaporation requires high-vacuum conditions, and the surface roughness is high. Alternatively, sputtering can improve both the surface roughness and the adhesion of the sputtered metal film to the substrate.

By combining metal-deposition technologies and the TPP technique, various metals, including gold, silver, copper, nickel, and alloys, can be coated onto the surfaces of prefabricated polymer structures, enabling the construction of various metallic structures with arbitrary shapes. Although great success has been achieved in metal structuring via surface coating, serious problems with respect to selective metal deposition still restrict their practical applications in efficient optical or electrical devices.

In this regard, selective metal coating onto polymeric structures is highly desired. Motivated by this goal, great efforts have been devoted to selective metal deposition. As a pioneering work, Kawata and co-workers achieved selective metallization by selective modification of the glass substrate and polymer structures with a hydrophobic coating and a layer of  $\text{SnCl}_2$  as an adhesion-promoting agent, respectively.<sup>[101,102]</sup> The hydrophobic coating on the glass could effectively hinder the silver plating, while the adhesion-promoting  $\text{SnCl}_2$  layer on the resin could increase silver nucleation and adhesion on the polymer surface. In this way, silver was selectively reduced only on the polymer surface, leaving the substrate clean. Importantly, the resistivity

of the resultant silver was measured to be  $\approx 8.2 \times 10^{-8}\ \Omega\text{ m}$ , only  $\approx 5$  times higher than that of bulk silver ( $1.6 \times 10^{-8}\ \Omega\text{ m}$ ).

In addition, Kuebler and co-workers developed an ingenious method for the selective coating of silver on complex 3D polymeric microstructures (Figure 5a).<sup>[103,104]</sup> This route is applicable to a broad range of polymers, such as acrylate, methacrylate, and epoxide resins. The polymer surface was first functionalized with alkylamines by  $\text{NH}_2(\text{CH}_2)_3\text{NHLi}$  treatment, which created surface-bound amine-terminated amides. Then, gold particles were bound to the pendant amines by immersing the structure in aqueous  $\text{AuCl}_4^-$  followed by reduction with  $\text{NaBH}_4$ . Next, highly conductive silver metal ( $1 \times 10^4\ \Omega^{-1}\text{ cm}^{-1}$ ) was selectively deposited onto the polymers by electroless plating and nucleated at the surface-bound gold nanoparticles. This metallization method is not limited to silver plating but is also feasible in the case of other metals. Later, selective copper coating onto SU-8 microstructures was achieved in a similar fashion,<sup>[88,105]</sup> demonstrating the universal nature of this approach.

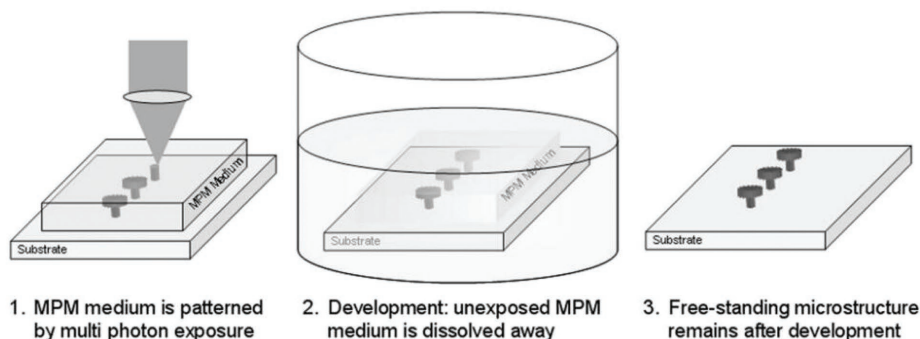
In addition to selective modification, Fourkas and co-workers developed a simple and highly selective metal-plating strategy by using two kinds of polymers with different reactivities, for instance, acrylic polymer and methacrylic polymer (Figure 5b).<sup>[50,106]</sup> Since the ethylene diamine reacted selectively with the acrylates by Michael addition, free amines were grafted onto the surface of the acrylic portion. The amines facilitated the formation of a catalytic palladium complex and enabled the selective electroless deposition of a range of different metals on the acrylic polymer. In this manner, selective metallization on desired regions of the acrylic polymer microstructures was achieved, leaving the methacrylic polymer surface unmetallized.

Notably, however, all the metallization approaches mentioned above suffer from the same problem. Prior to the electroless plating procedure, a surface activation step is always necessary, and thus, the subsequent metallization relies largely on the surface-functionalization process. Moreover, the density of the metal-binding sites on the polymers formed during this metal-plating process is difficult to control, especially in the case of complex 3D structures. Thus, inhomogeneous metal deposition occurs in most cases. Obtaining uniformly metallized structures in a controllable fashion remains a challenge. Toward this end, Farsari and co-workers reported an alternative approach, which employed the 3D structuring and metallization of a zirconium-based organic–inorganic photosensitive material pre-doped with metal-binding tertiary amine moieties.<sup>[107,108]</sup> In this way, selective metallization was achieved because the binding sites existed only on the polymers, leaving the substrate completely unactivated.

### 2.2.2. Template-Assisted Metal Filling

Despite the abovementioned successes, many problems still restrict the practical application of fabricating freestanding metallic devices, particularly truly 3D configurations. Regardless of the photoreduction of metal ions in polymer matrixes or the subsequent coating of metal onto polymer surfaces, obtaining solid metal structures with sufficient mechanical strength is difficult because the interior polymers are often

**(a) Multi photon 3D Microfabrication (MPM)**



**Silver Deposition**

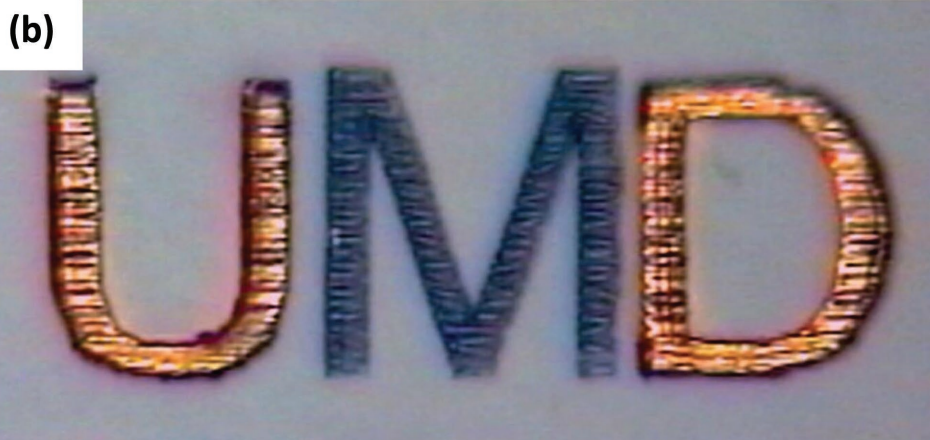
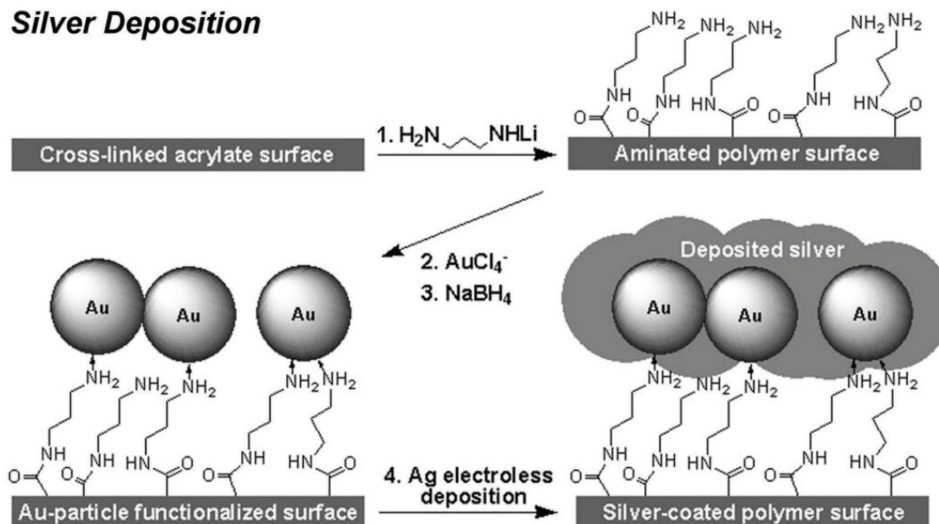


**Figure 5.** Representation of metal coating on polymer templates prefabricated by laser direct writing. a) Schematic illustration of the process for creating silver–polymer microstructures. First, a polymeric template is fabricated by TPP using acrylate resin. Next, the surface of the microstructure template is aminated with  $\text{NH}_2(\text{CH}_2)_3\text{NHLi}$ , thus enabling  $\text{Au}^{3+}$  to bind at the amine sites and subsequently be reduced with  $\text{NaBH}_4$ . Finally, electroless plating is employed to apply a silver coating nucleated at surface-bound gold particles. Reproduced with permission.<sup>[103]</sup> Copyright 2006, Wiley-VCH. b) Selective metallization of microstructures achieved by selective copper deposition on the preferred polymer surface (acrylic polymer). The “U” and “D” labels represent acrylic polymer, and “M” represents methacrylic polymer. Reproduced with permission.<sup>[50]</sup> Copyright 2007, Wiley-VCH.

prone to shrink or collapse. To address this issue, Wegener and co-workers proposed a template-assisted metal-filling method that involved processing a positive-tone photoresist followed by electrochemical metal deposition.<sup>[109–113]</sup> Later,

Greer and co-workers further extended this strategy to the fabrication of 3D interconnected microstructures, the schematic illustration of which is shown in **Figure 6a**.<sup>[114]</sup> Electrochemical deposition is a process that uses an electric current

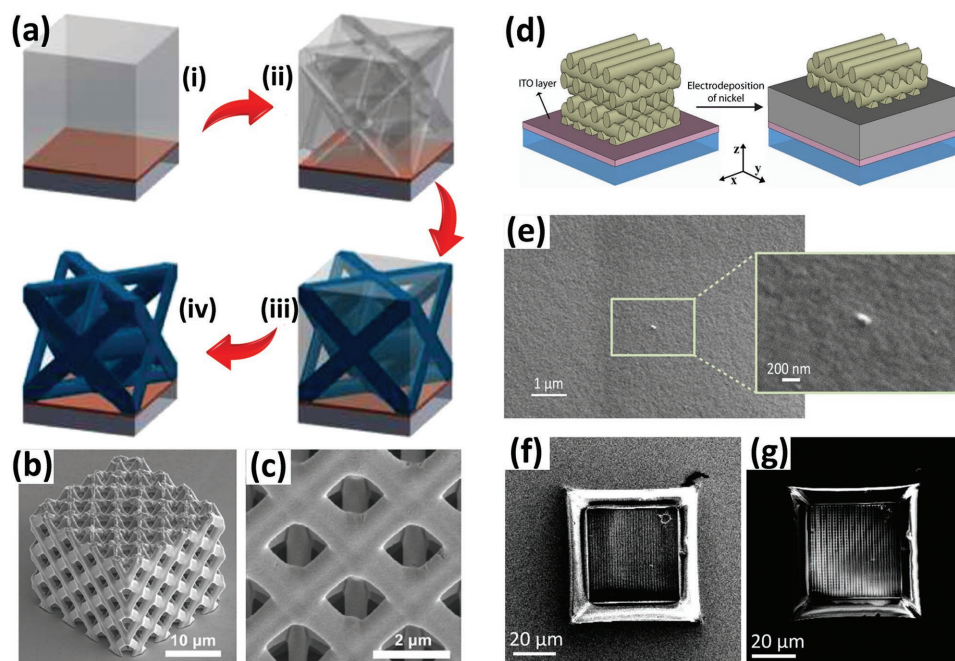


**Figure 6.** Examples of producing metallic structures through metal filling into prefabricated templates created by laser direct writing. a) Schematic diagram of the fabrication procedure using a positive photoresist: i) spin coating the positive photoresist onto an ITO-covered glass substrate, ii) FSLDW of the 3D pattern into the photoresist, iii) electroplating of the metal into the pores, and iv) removing the photoresist to leave behind the solid metallic structures. b, c) SEM images of the obtained copper octet mesolattices. a–c) Reproduced with permission.<sup>[114]</sup> Copyright 2015, Elsevier. d) Scheme for the fabrication procedure of inverse metallic woodpile photonic crystals. Metal is infiltrated into the woodpile photoresist template via the electrodeposition of nickel. e) SEM images of the electrodeposited nickel film on an ITO-covered glass substrate. f) SEM image of the nickel-infiltrated woodpile microstructure. g) High-contrast SEM image that exhibits the top layers of the woodpile microstructure. d–g) Reproduced with permission.<sup>[115]</sup> Copyright 2012, Optical Society of America.

to reduce metal ions so that they can form a coherent metal coating on a conductive substrate, and this technique has been widely adopted for the growth of metals due to several distinct advantages. First, the thickness and morphology of the deposited metal nanostructure can be precisely controlled by adjusting the deposition conditions. Second, relatively uniform and compact deposits can be obtained in template-based structures. Third, electrochemical deposition can produce various metals such as gold, silver, copper, nickel, and so on. By using positive-tone photoresists, any desired void channels with predesigned architectures can be easily fabricated as templates. Since the hollow template can be completely filled with metal by electrodeposition, solid metallic microstructures can be fabricated by removing the photoresist using oxygen plasma etching. By using this fabrication strategy, a freestanding 3D copper octet mesolattice structure was successfully created via copper infiltration into the air channels fabricated by FSLDW (Figure 6b,c).

Nevertheless, the metal-filling method is feasible only for the fabrication of simple 3D structures, and problems emerge when making metallic structures with more complex shapes, for instance, woodpile configurations. The technical challenge is that during the metal-filling process, certain parts of the horizontally aligned void cavities are cut off from the electrodeposition solution before being fully filled, thus leaving gaps in the final metal structure. For this reason, the fabrication of woodpile metallic microstructures remains a challenge. However, the most relevant study with regard to this knotty problem was

conducted by Gu and co-workers (Figure 6d).<sup>[115]</sup> They obtained a 3D metallic woodpile microstructure by using FSLDW in a negative-tone photoresist followed by nickel electrodeposition. The surface morphology of the deposited nickel film is demonstrated in Figure 6e, and scanning electron microscopy (SEM) images of the acquired inverse woodpile nickel photonic crystal are shown in Figure 6f,g. The 3D woodpile skeleton was fabricated first, and then nickel was deposited to form an inverse woodpile metallic structure. In this work, removing the polymer part for the creation of solid metal structures was challenging. In addition, the obtained metallic configuration had the inverse geometry of the predesigned polymer woodpile microstructure. Despite these problems, this method has proven useful, since it may enable the realization of 3D metallic photonic crystals with intriguing optical properties that cannot be obtained from alternative techniques.

To obtain pure metallic micro/nanostructures, it is highly desirable to remove the polymeric templates. In the metal-filling technique, the photoresist template wrapped outside the metal can be easily etched away by oxygen plasma treatment.<sup>[109]</sup> However, in the case of metal coated outside the polymer, the template cannot simply be removed in the same manner. To solve this problem, Greer and co-workers proposed a very innovative approach.<sup>[98–100]</sup> By milling the two sides of the structure with a focused ion beam, the interior polymer was exposed to the environment, allowing the inside polymer template to be successfully etched away using oxygen plasma, providing a very effective strategy for template removal.

### 2.3. Femtosecond-Laser Photodynamic Assembly of Metal Nanoparticles

By exploiting the optical-trapping effect,<sup>[116–122]</sup> FsLDW also enables the direct assembly of metallic nanoparticles into desired microstructures through the “femtosecond-laser photodynamic assembly (FsL-PDA)” process (depicted in Figure 1c). Using metal nanoparticles as nano-building-blocks, Sun and co-workers first achieved the FsL-PDA of metallic microstructures.<sup>[123,124]</sup> At the laser focus, the nanoparticles could be trapped by the local potential wells produced by the laser beam and then subsequently assembled according to pre-designed patterns. In fact, the potential wells could be considered as microtweezers that can precisely control the assembly of nanoparticles. As a typical example, Wang et al. successfully assembled silver nanoparticles with an average particle size of  $\approx 2.5$  nm into various patterns using the FsL-PDA technique (Figure 7).<sup>[123]</sup> By adjusting the laser power or exposure time, silver nanowires with varying widths could be obtained, and a resolution as high as 190 nm was obtained (shown in Figure 7c). The magnified SEM images in Figure 7d demonstrate that the silver nanostructures were constructed by closely packed nanoparticles. Owing to the flexible fabrication and integration ability of the FsL-PDA technique, microelectrodes, microheaters, and catalytic reactors can be integrated into a microfluidic channel for chip functionalization. In addition, Xu et al. fabricated gold microstructures by adopting gold nanoparticles as the precursor solution.<sup>[124]</sup> The electrical resistivity of the as-formed gold patterns could reach  $5.5 \times 10^{-8} \Omega \text{ m}$ , which was only twice that of the bulk material ( $2.4 \times 10^{-8} \Omega \text{ m}$ ). At

present, the FsL-PDA method remains in its infancy, and many problems exist. Currently, the assembly of 3D structures by this technique remains difficult, which could be ascribed to two underlying factors: the effect of LSPR caused by metal nanoparticles and the relatively low concentration of nanoparticles in the local focus spot. Generally, the formation of metal structures, such as silver or gold, can cause LSPR, which may further influence the subsequent assembly of nanoparticles, thus hindering the creation of 3D structures. To obtain a certain transmittance of the laser beam, the concentration of the metal nanoparticle precursor cannot be too high. Therefore, the quantity of nanoparticles in the laser focus spot is often insufficient for the creation of 3D constructions.

### 2.4. Femtosecond-Laser Selective Nanoparticle Sintering

Another novel method enabling the fabrication of metal microstructures is direct femtosecond-laser selective nanoparticle sintering (FLSNS) (depicted in Figure 1d). As is well known, because of the thermodynamic size effect,<sup>[125,126]</sup> the melting temperature of metal nanoparticles can be reduced to as low as 100–200 °C. If an ultrashort femtosecond laser is used as a local heat source for selective nanoparticle melting, the prepared metal-nanoparticle film can be selectively melted by scanning the focused laser beam. After this process, the remaining unmelted nanoparticles can be washed away by organic solvent, leaving only the laser-processed micropatterns. Due to the ultrashort nature of the femtosecond laser, the thermal effect is significantly reduced, and the diffraction limit can be overcome. A

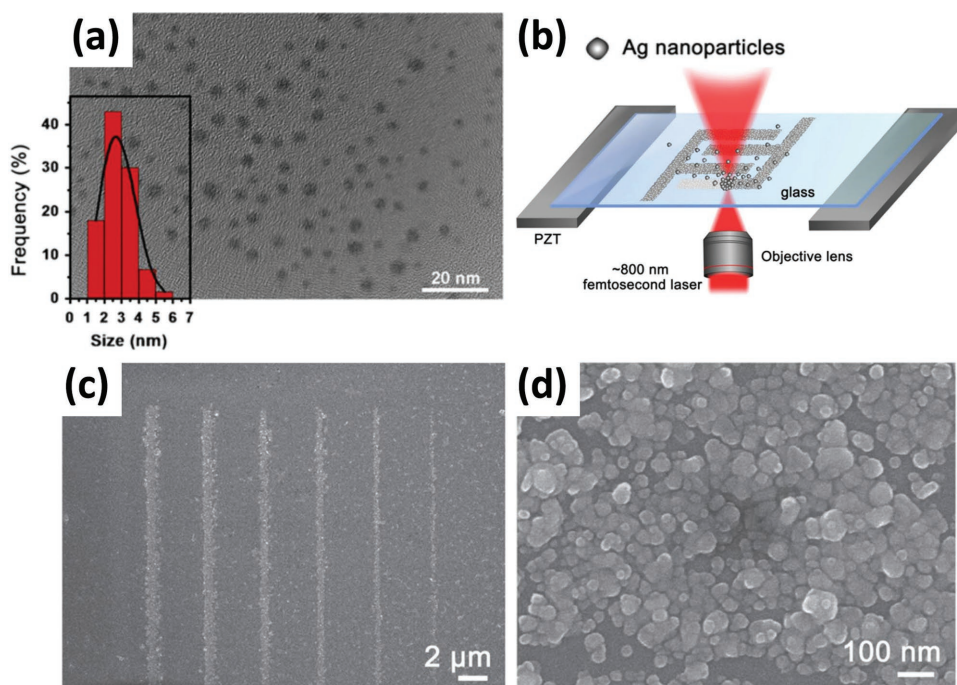


**Figure 7.** Patterning of silver nanostructures by the FsL-PDA of silver nanoparticles. a) TEM image of the silver nanoparticles used. The inset diagram shows the particle size distribution with an average diameter of  $\approx 2.5$  nm. b) Schematic illustration of the controllable assembly process of silver nanoparticles. c) Silver wires with different widths created by varying the laser intensity. d) Magnified SEM image of the patterned silver nanostructures. Reproduced with permission.<sup>[123]</sup> Copyright 2015, Institute of Physics.

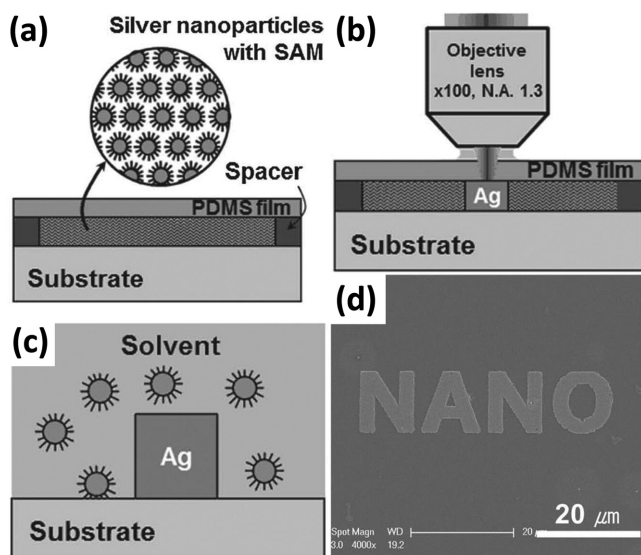


**Figure 8.** Scheme for the femtosecond-laser selective nanoparticle sintering process. a) Silver-nanoparticle ink was spin coated onto a glass substrate to form a nanoparticle thin film. b) The prepared thin film was selectively sintered by femtosecond-laser scanning. c) After laser processing, the untreated silver nanoparticles were washed away by organic solvent, leaving only the laser-sintered metals. d) SEM image of the “NANO” pattern produced by the laser sintering of silver nanoparticles. Reproduced with permission.<sup>[127]</sup> Copyright 2011, Wiley-VCH.

representative example of this method was reported by Ko and co-workers (Figure 8).<sup>[127]</sup> In their study, silver-nanoparticle ink was spin-coated onto a cover glass or a silicon wafer substrate to form a nanoparticle thin film. Uniform silver lines with a minimum width of 380 nm could be obtained after the FLSNS process, demonstrating the high-resolution patterning ability. The resistivity was measured to be as low as  $1.8 \times 10^{-5} \Omega \text{ cm}$ , which was nearly eleven times higher than that of bulk silver ( $1.59 \times 10^{-6} \Omega \text{ cm}$ ). Using the FLSNS technique, other metal nanoparticles, such as copper, could be patterned,<sup>[128]</sup> which may be of great use for copper interconnection technology in microelectronics. Due to limitations in the transmittance of the laser beam, the thickness of the metal nanoparticle ink film should usually be relatively thin, and thus, this method is limited to the fabrication of 2D metallic patterns.

### 3. Broad Applications

By taking advantage of FsLDW technology, various 3D metallic micro/nanostructures with preprogrammed 3D architectures can be readily fabricated, which has sparked considerable research interest in applying these metallic structures in various scientific fields, such as microelectronics, metamaterials, near-field optics, microfluidics, micromechanics, and microsensors (displayed in Figure 1e–i).

In microelectronics (Figure 1e), conductive microstructures are highly desired. In a typical study, Fourkas and co-workers successfully produced a 16-turn copper coil inductor 200  $\mu\text{m}$  in length and 24  $\mu\text{m}$  in diameter by using the selective electroless copper plating strategy (Figure 9).<sup>[106]</sup> These electrical

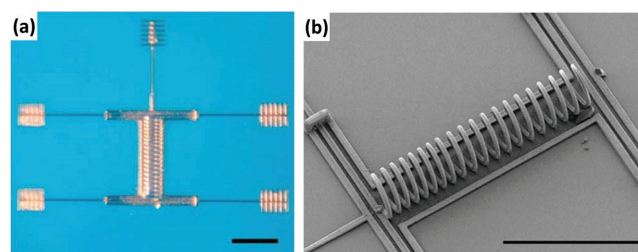


**Figure 9.** Application of the FsLDW of metallic micro/nanostructures in microelectronics. a) Optical microscopy image, and b) SEM image of a 3D 16-turn microinductor coil 200  $\mu\text{m}$  in length and 24  $\mu\text{m}$  in diameter. Scale bars: 100  $\mu\text{m}$ . Reproduced with permission.<sup>[52]</sup> Copyright 2007, Elsevier.

devices are of great importance in communication, including in the fields of filters, transformers, and oscillator circuits. Such inductors involve a high demand for 3D fabrication capability and are therefore quite challenging for common technologies. However, FsLDW technology makes this type of fabrication easy. Moreover, FsLDW also permits metal nanowiring for electronic interconnection on nonplanar substrates, which is almost impossible for traditional lithography.<sup>[60,73]</sup> Sun and co-workers realized the flexible nanowiring of silver on nonplanar substrates by the femtosecond laser-induced direct two-photon reduction of  $\text{Ag}(\text{NH}_3)_2^+$  in the presence of trisodium citrate.<sup>[60]</sup> As a representative demonstration, a single silver wire circle passing over the frustums of the pyramids was created, revealing great potential for 3D electrical interconnection or the flexible integration of microcircuits. Due to its flexible, designable, and site-selective patterning capability, FsLDW has been used to produce metal nanowiring to fabricate metal microelectrodes in working devices.<sup>[124,127,129]</sup> In a representative study where high-performance field-effect transistors (FETs) were fabricated, a nanotube located between the source and drain electrodes was successfully connected to the S/D electrodes to produce an FET by the FsL-PDA of gold nanoparticles.<sup>[124]</sup>

In addition to electronics, FsLDW is also promising for the designable manufacture of metallic structures as metamaterials (Figure 1f). The burgeoning field of metamaterials has seen many ground-breaking theoretical and experimental advances in recent years, resulting in a new milestone with regard to the development of electromagnetic science. Metamaterials derive their properties mainly from their micro/nanostructures, including their precise shape, geometry, size, orientation, and arrangement instead of their intrinsic material properties. Thus, metamaterials are capable of manipulating electromagnetic waves; by blocking, absorbing, enhancing, or bending waves, they can achieve benefits beyond what is possible with conventional materials that exist in nature. Because of its flexible and maskless patterning capability, FsLDW can be employed to fabricate 2D metallic features for metamaterial design. Tanaka and co-workers demonstrated a metamaterial consisting of a 2D silver rod pair array constructed by the TPA-induced reduction of metal ions.<sup>[130]</sup> The magnetic resonance response was clearly observed with a negative permeability around the resonant frequency of 16.77 THz. In addition, Duan and co-workers fabricated 2D arrays of U-shaped gold split-ring resonators by the direct two-photon reduction of  $\text{AuCl}_4^-$  ions

in aqueous solution, demonstrating an electric resonance of  $\approx 63$  THz for a specific polarization.<sup>[68]</sup>

Metamaterials fabricated via FsLDW are not limited to 2D planar structures; by combining FsLDW fabrication with subsequent silver CVD, Wegener and co-workers took the first step toward a truly 3D magnetic metamaterial operating at near-infrared frequencies.<sup>[2]</sup> After careful design of the geometrical shape, the magnetic permeability  $\mu$  exhibited a magnetic resonance with  $\text{Re}(\mu) < 0$  in a certain frequency range, demonstrating the successful development of a magnetic metamaterial. Another representative 3D metamaterial is the polarization-dependent perfect absorber/reflector proposed by Wang and co-workers.<sup>[97]</sup> A 3D standing U-shaped metamaterial was fabricated by the magnetron sputtering of gold onto 3D polymer microstructures created beforehand via FsLDW. For selective polarization, the structures could act as a perfect absorber, and when the polarization was rotated by  $90^\circ$ , the incident light could be reflected perfectly, as from a mirror. This kind of structure is highly useful for controlling or detecting the polarization of light.

Chiral metamaterials, which are inherently a 3D phenomenon, may present various intriguing optical effects, such as gyrotropy,<sup>[131]</sup> circular dichroism,<sup>[132]</sup> and negative phase velocities.<sup>[133]</sup> Wegener and co-workers performed an innovative study on the propagation of light through a uniaxial metamaterial composed of 3D gold helices fabricated by FsLDW and electrodeposition.<sup>[109]</sup> Interestingly, for normal incidence light, the circular polarization with the same handedness as the helices was blocked, while the opposite polarization was able to transmit along the helix axis, which operated in the wavelength range of  $3.5\text{--}7.5\ \mu\text{m}$ , thus serving as a broadband circular polarizer. To obtain a larger bandwidth and extinction ratio, they created improved devices using a tapered gold helix configuration.<sup>[110]</sup> Despite the advantages of helical metamaterials with regard to bandwidth and extinction ratio, their practical application is limited due to circular-polarization conversions. In a subsequent study, a new model  $N$ -helix metamaterial ( $N = 3$  or  $4$ ) was introduced (Figure 10).<sup>[111]</sup> By intertwining three or four helices within each unit cell, the circular-polarization conversions could be largely minimized throughout most of the operation band, as undesired polarization was absorbed instead of simply being reflected. By making full use of FsLDW, various functional metamaterial structures have been successfully produced, especially 3D configurations, which are tremendously important and useful for novel device designs that cannot be realized by conventional micro/nanofabrication strategies. In this regard, the FsLDW technique holds great promise for the development of novel 3D metamaterials.

In near-field optics (Figure 1g), the FsLDW of metallic micro/nanostructures also plays a very important role. The SERS technique has attracted much attention because it can directly provide fingerprint information on various target molecules, and thus allows the highly sensitive detection of analytes at very low concentrations, even at the single-molecule level.<sup>[14–18]</sup> The enhancement of the electromagnetic field for SERS relies heavily on the LSPR derived from the metal nanostructures.<sup>[23,134]</sup> Thus, the fabrication of metallic micro/nanostructures that are of benefit to LSPR is essential for the development of highly efficient SERS substrates. The FsLDW technique has been adopted

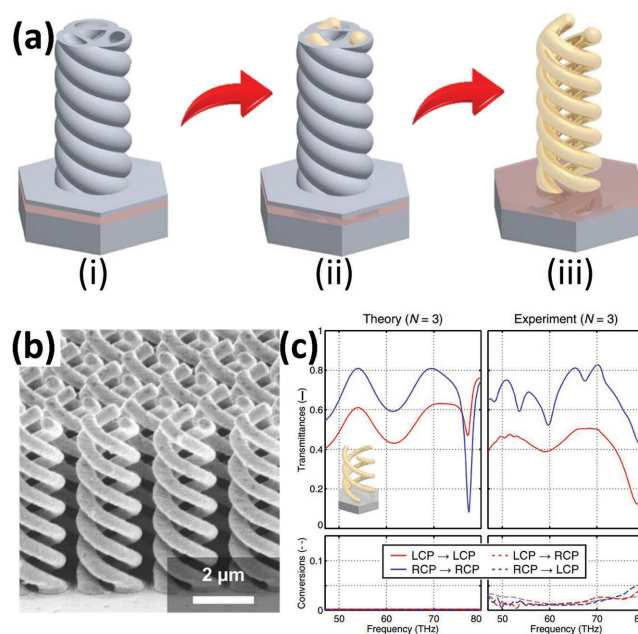


**Figure 10.** Application of the FsLDW of metallic micro/nanostructures in metamaterials. a) Fabrication procedures for a 3D gold triple-helix array: i) FsLDW of the 3D helix pattern into the photoresist, ii) infiltration of gold into the hollow template by electroplating, and iii) removal of the polymer template to obtain the gold solid helix structure. b) SEM image of an array of gold intertwining helices. c) Simulated and measured spectra of the Jones transmission matrix for helical metamaterials. The polarization-conserving transmittance and the polarization conversion are depicted by the solid and dashed lines, respectively. Reproduced with permission.<sup>[111]</sup> Copyright 2015, Optical Society of America.

for the production of SERS substrates because it enables the designable structuring of several SERS active metals, such as silver and gold.<sup>[135–139]</sup> By employing the direct two-photon reduction of silver ions in aqueous solution, Xu et al. fabricated hierarchical silver substrates consisting of vertical silver nanoplates and nanoparticles decorated on each silver plate, which were used as SERS substrates, thereby achieving high SERS enhancement (Figure 11a–c).<sup>[135]</sup> In addition, FsLDW enables the integration of SERS substrates with other functional devices or systems. For example, SERS substrates have been fabricated directly on fiber tips or inside microfluidic chips. In this way, simple, highly efficient and high-throughput SERS measurements have been achieved.

The fabrication and integration of metallic micro/nanostructures also contributes to microfluidics (Figure 1h). In particular, with the gradually increasing requirements of lab-on-a-chip (LoC) systems,<sup>[140]</sup> the integration of functional microstructures at desired positions on a microfluidic chip is of great importance. However, this task is highly challenging for traditional technologies such as lithography or imprinting, since the surface of microfluidic devices is usually not flat. With its programmable 3D fabrication capability, FsLDW can solve this problem very well. As a typical example, Sun and co-workers reported the flexible integration of high-efficiency SERS monitors into microfluidic chips by employing the direct two-photon reduction of silver ions in aqueous solution.<sup>[135]</sup> SERS substrates can be patterned into various shapes and precisely located at

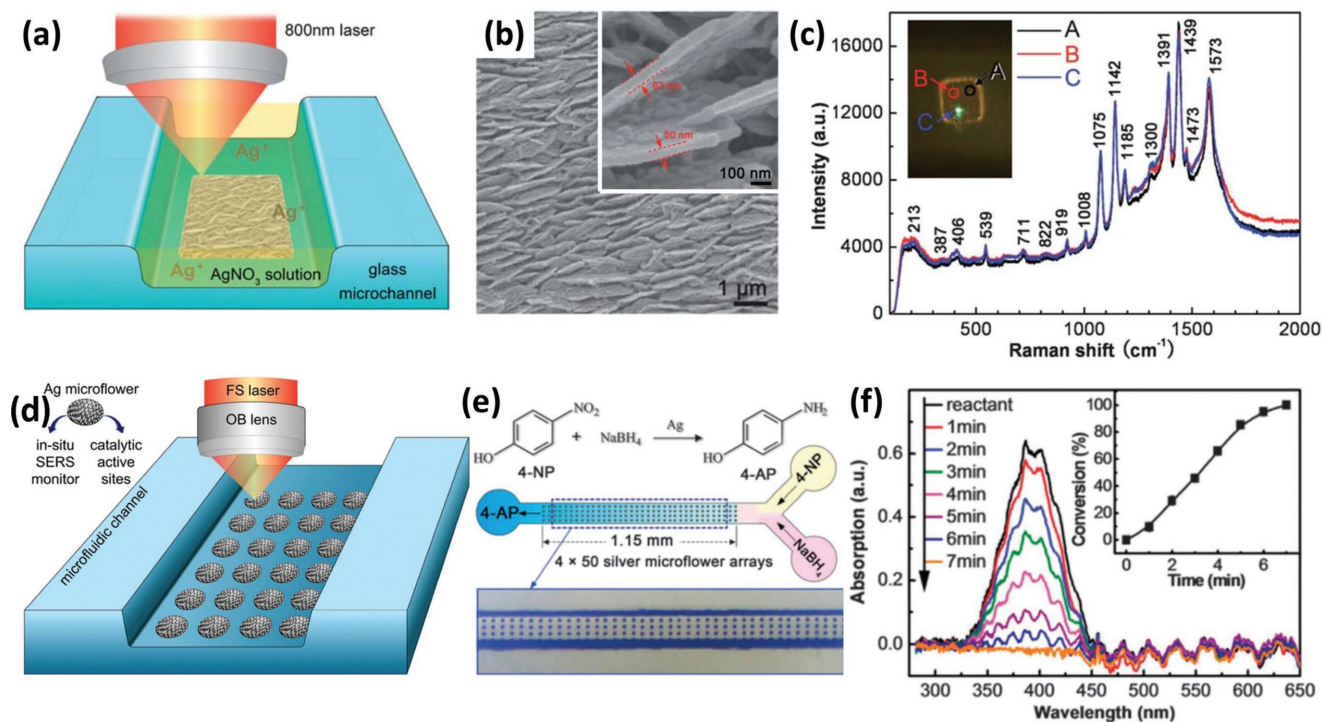


**Figure 11.** Application of the FSLDW of metallic micro/nanostructures in a–c) near-field optics and d–f) microfluidics. a) Schematics for the fabrication of silver SERS substrates by the two-photon reduction of silver ions in solution. b) SEM images of SERS substrates composed of vertical silver nanoplates. The inset shows the magnified SEM image of the rough surface. c) The measured SERS spectra using p-aminothiophenol as the molecular probe. Reproduced with permission.<sup>[135]</sup> Copyright 2011, The Royal Society of Chemistry. d) Schematic illustration of the integration of catalytic SMAs inside a microfluidic channel. e) Optical microscopy image of the microfluidic channel integrated with SMAs as catalytic sites for the reduction of 4-NP to 4-AP. f) Absorption spectra of the microfluids after reaction for several minutes with an interval of 1 min. The inset shows the kinetic study of this catalytic reaction. Reproduced with permission.<sup>[19]</sup> Copyright 2012, The Royal Society of Chemistry.

any desired position in the microchannel, achieving the real-time detection of on-chip chemical reactions. In addition, the integration of metallic micro/nanostructures with microfluidic chips enables on-chip catalysis.<sup>[19–21,123,141]</sup> For instance, Sun and co-workers fabricated silver-microflower arrays (SMAs) as robust catalytic sites for the reduction of 4-nitrophenol (4-NP) to 4-aminophenol (4-AP) (Figure 11d–f).<sup>[19]</sup> Notably, the SMAs serve not only as catalysts but also as highly efficient SERS substrates, enabling in situ SERS monitoring of the catalytic reaction. Later, Kaehr and co-workers reported the integration of catalytic Pd and Pt microstructures within a 3D microfluidic environment through the direct two-photon reduction of palladium ions and platinum ions in aqueous solution.<sup>[20]</sup> Site-specific  $H_2O_2$  decomposition catalyzed by nanocrystalline Pt or Pd could be used to drive directed fluid flow in 3D, which may be useful for site-specific catalysis in microfluidic systems by enabling flow generation, fluid mixing, propulsion, collection, and transport. Compared with traditional fabrication technologies adopted for microfluidic-chip functionalization, femtosecond-laser fabrication exhibits several unique advantages. For example, it enables the programmable fabrication of metallic micro/nanostructures with a predesigned shape, size, and location. FSLDW technology is compatible with microfluidic chips that are not flat. More importantly, FSLDW is a 3D technique and thus holds great promise for the integration of more complex metallic micro/nanostructures for chip functionalization.

In addition to the abovementioned applications, the fabrication of metal structures via FSLDW has also demonstrated potential in various scientific fields, such as micromechanics (Figure 1i),<sup>[85,86,93–96]</sup> and microsensors.<sup>[69]</sup> For instance, by applying electroless copper plating on a prefabricated polymer template, Maruo and co-workers fabricated 3D metallic movable microparts, such as a microrotor and a microscrew, which could potentially be used in MEMS or LoC systems.<sup>[86]</sup> Duan and co-workers prepared 3D micromachines by combining FSLDW and the electroless plating of nickel-phosphorus.<sup>[85]</sup> Zhang and co-workers fabricated magnetic helical micromachines using FSLDW and the electron-beam evaporation of nickel (Figure 1j).<sup>[93]</sup> The resulting helical microrobots were capable of performing steerable corkscrew motions at high speed in 3D, exhibiting great potential for the micromanipulation of biological cells or in vivo drug delivery. In addition, Qu and co-workers reported the fabrication of hydrogen ( $H_2$ ) sensors based on palladium patterns fabricated by the femtosecond-laser direct two-photon reduction of palladium acetate.<sup>[69]</sup>

#### 4. Conclusion and Outlook

We have summarized recent developments in the field of metallic micro/nanostructures from the perspective of femtosecond-laser fabrication strategies and their wide applications.



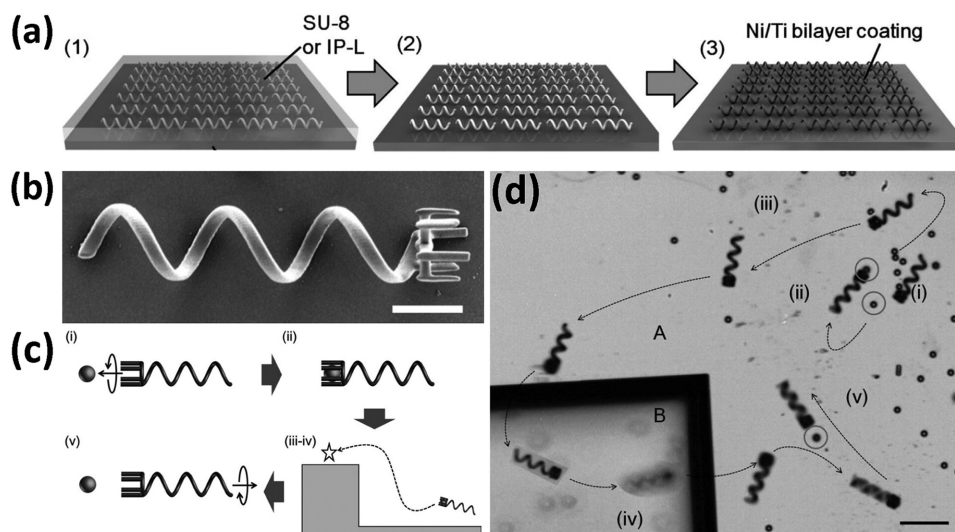


**Figure 12.** Application of the FSLDW of metallic micro/nanostructures in micromechanics. a) Schematic for the fabrication of helical swimming micromachines: 1) FSLDW of helical patterns into the photoresist, 2) removal of the unpolimerized photoresist after developing, and 3) deposition of Ni/Ti on the surface of the polymer helical micromachine by electron-beam evaporation. b) The helical micromachine with a finger-like microholder. Scale bar: 10  $\mu\text{m}$ . c) Schematic demonstration of the transportation procedure using the helical micromachine with a microholder. d) Time-lapse image of the cargo transport of a particle 6  $\mu\text{m}$  in diameter in deionized water. Scale bar: 50  $\mu\text{m}$ . Reproduced with permission.<sup>[93]</sup> Copyright 2012, Wiley-VCH.

As a powerful fabrication tool, FSLDW allows the designable fabrication and integration of metallic micro/nanostructures through several strategies, such as the TPA-induced direct photoreduction of metal ions, template-assisted metal coating or filling, photodynamic assembly of metal nanoparticles, and laser sintering of metal nanoparticles. Furthermore, the applications of FSLDW-fabricated structures in several dynamic research fields, including microelectronics, metamaterials, near-field optics, microfluidics, micromechanics, and micro-sensors, are summarized. Compared with conventional micro/nanofabrication technologies, especially those focusing on metal structuring, the FSLDW technique offers several distinct advantages, such as designable processing without the use of masks, ease of integration with given devices, and feasibility of 3D structuring capability.

At present, although great success has already been achieved in the FSLDW of metallic micro/nanostructures, new photochemical or photophysical schemes that enable more sophisticated fabrication are urgently needed, offering a large scope for development, as several problems still hamper the broad applications of these structures. Currently, the creation of true 3D solid metallic structures with high conductivity through FSLDW alone remains a challenge. Although template-assisted metal coating or filling approaches can produce 3D metallic structures, these methods also suffer from the serious problem of structure shrinkage during the removal of polymer templates and are limited to the fabrication of several simple configurations. Additionally, the roughness of the metallic structures produced by FSLDW-induced photoreduction remains unsatisfactory owing to the mass diffusion effect during the fabrication process, which can lead to severe optical loss or a significant decrease in the electrical conductivity. These issues are critical and restrict the applications of currently fabricated structures in optical and electrical elements. Moreover, the resolution of the obtained metallic

features needs to be further improved. Based on the state of the art of this technology, the current resolution can reach  $\approx 120$  nm when fabricating a single metallic line. However, in this case, the metallic patterns become almost discontinuous. As a consequence, the electrical conductivity is greatly reduced or sacrificed, thus hampering the practical applications of the structures in electronics or optical metamaterials that require ultrafine metallic features. Therefore, improving the resolution while maintaining relatively high conductivity is an urgent challenge that should be addressed as soon as possible. By using metal nanoparticles as nano-building-blocks, the FSLDW-induced photodynamic assembly technology, which enables the trapping and manipulation of nanomaterials, has the potential to achieve this goal. However, to achieve nanoscale resolution or 3D metallic configuration, uniform metal nanoparticles must first be prepared. More importantly, since the as-formed metallic structures produce LSPR under laser excitation, the influence of the local electromagnetic field should be considered.

In short, femtosecond-laser technology plays an important role in the fabrication and application of metallic micro/nanostructures. With the rapid development of new processing strategies, the fabrication of metallic micro/nanostructures with arbitrary shapes, improved roughness and high resolution may be realized shortly. Undoubtedly, with the support of FSLDW technology, metallic micro/nanostructures will find increasingly broad applications in both scientific research and practical use in the near future.

## Acknowledgements

This work was supported by the National Key Research and Development Program of China and National Natural Science Foundation of China (NSFC) under Grants #2017YFB1104300, #61522503, #61775078, #61590930 and #61435005.

## Conflict of Interest

The authors declare no conflict of interest.

## Keywords

femtosecond-laser direct writing, metallic microstructures, nanofabrication, photochemistry, photoreduction

Received: December 21, 2017

Revised: January 26, 2018

Published online:

- [1] D. Wen, F. Yue, G. Li, G. Zheng, K. Chan, S. Chen, M. Chen, K. F. Li, P. W. Wong, K. W. Cheah, E. Y. Pun, S. Zhang, X. Chen, *Nat. Commun.* **2015**, *6*, 8241.
- [2] M. S. Rill, C. Plet, M. Thiel, I. Staude, G. von Freymann, S. Linden, M. Wegener, *Nat. Mater.* **2008**, *7*, 543.
- [3] X. Yin, T. Steinle, L. Huang, T. Taubner, M. Wuttig, T. Zentgraf, H. Giessen, *Light: Sci. Appl.* **2017**, *6*, e17016.
- [4] Y. Imade, R. Ulbricht, M. Tomoda, O. Matsuda, G. Seniutinas, S. Juodkazis, O. B. Wright, *Nano Lett.* **2017**, *17*, 6684.
- [5] D. Hakobyan, H. Magallanes, G. Seniutinas, S. Juodkazis, E. Brasselet, *Adv. Opt. Mater.* **2016**, *4*, 306.
- [6] C. Shan, F. Chen, Q. Yang, Y. Li, H. Bian, J. Yong, X. Hou, *Opt. Lett.* **2015**, *40*, 4050.
- [7] N. Y. Kim, K. K. Adhikari, R. Dhakal, Z. Chuluunbaatar, C. Wang, E. S. Kim, *Sci. Rep.* **2015**, *5*, 7807.
- [8] B. Frank, P. Kahl, D. Podbiel, G. Spektor, M. Orenstein, L. Fu, T. Weiss, M. Horn-von Hoegen, T. J. Davis, F.-J. M. zu Heringdorf, H. Giessen, *Sci. Adv.* **2017**, *3*, e1700721.
- [9] T. Oshikiri, K. Ueno, H. Misawa, *Angew. Chem., Int. Ed.* **2016**, *55*, 3942.
- [10] Q. Sun, H. Yu, K. Ueno, A. Kubo, Y. Matsuo, H. Misawa, *ACS Nano* **2016**, *10*, 3835.
- [11] O. Lecarme, Q. Sun, K. Ueno, H. Misawa, *ACS Photonics* **2014**, *1*, 538.
- [12] M. Hentschel, M. Schaferling, X. Y. Duan, H. Giessen, N. Liu, *Sci. Adv.* **2017**, *3*, e1602735.
- [13] Q. Sun, K. Ueno, H. Yu, A. Kubo, Y. Matsuo, H. Misawa, *Light: Sci. Appl.* **2013**, *2*, e118.
- [14] L. K. Shrestha, M. Sathish, J. P. Hill, K. i. Miyazawa, T. Tsuruoka, N. M. Sanchez-Ballester, I. Honma, Q. Ji, K. Ariga, *J. Mater. Chem. C* **2013**, *1*, 1174.
- [15] G. Seniutinas, G. Gervinskas, R. Verma, B. D. Gupta, F. Lapierre, P. R. Stoddart, F. Clark, S. L. McArthur, S. Juodkazis, *Opt. Express* **2015**, *23*, 6763.
- [16] Y. Huang, Y. Fang, Z. Zhang, L. Zhu, M. Sun, *Light: Sci. Appl.* **2014**, *3*, e199.
- [17] Y. Yokota, K. Ueno, H. Misawa, *Small* **2011**, *7*, 252.
- [18] H. Jung, M. Park, M. Kang, K.-H. Jeong, *Light: Sci. Appl.* **2016**, *5*, e16009.
- [19] B. B. Xu, R. Zhang, X. Q. Liu, H. Wang, Y. L. Zhang, H. B. Jiang, L. Wang, Z. C. Ma, J. F. Ku, F. S. Xiao, H. B. Sun, *Chem. Commun.* **2012**, *48*, 1680.
- [20] L. D. Zarzar, B. S. Swartzentruber, J. C. Harper, D. R. Dunphy, C. J. Brinker, J. Aizenberg, B. Kaehr, *J. Am. Chem. Soc.* **2012**, *134*, 4007.
- [21] B.-B. Xu, Y.-L. Zhang, S. Wei, H. Ding, H.-B. Sun, *ChemCatChem* **2013**, *5*, 2091.
- [22] Q. Ji, J. P. Hill, K. Ariga, *J. Mater. Chem. A* **2013**, *1*, 3600.
- [23] M. Rycenga, C. M. Cobley, J. Zeng, W. Li, C. H. Moran, Q. Zhang, D. Qin, Y. Xia, *Chem. Rev.* **2011**, *111*, 3669.
- [24] C. Zhu, D. Du, A. Eychmuller, Y. Lin, *Chem. Rev.* **2015**, *115*, 8896.
- [25] M. A. Boles, M. Engel, D. V. Talapin, *Chem. Rev.* **2016**, *116*, 11220.
- [26] A. Walther, A. H. Muller, *Chem. Rev.* **2013**, *113*, 5194.
- [27] M. Gschrey, A. Thoma, P. Schnauber, M. Seifried, R. Schmidt, B. Wohlfeil, L. Kruger, J. H. Schulze, T. Heindel, S. Burger, F. Schmidt, A. Strittmatter, S. Rodt, S. Reitzenstein, *Nat. Commun.* **2015**, *6*, 7662.
- [28] B. Radha, G. U. Kulkarni, *Adv. Funct. Mater.* **2012**, *22*, 2837.
- [29] A. Cui, Z. Liu, J. Li, T. H. Shen, X. Xia, Z. Li, Z. Gong, H. Li, B. Wang, J. Li, H. Yang, W. Li, C. Gu, *Light: Sci. Appl.* **2015**, *4*, e308.
- [30] B. Sain, R. Kaner, Y. Prior, *Light: Sci. Appl.* **2017**, *6*, e17072.
- [31] M. A. Skylar-Scott, S. Gunasekaran, J. A. Lewis, *Proc. Natl. Acad. Sci. USA* **2016**, *113*, 6137.
- [32] R. D. Farahani, M. Dube, D. Theriault, *Adv. Mater.* **2016**, *28*, 5794.
- [33] E. C. Spivey, E. T. Ritschdorff, J. L. Connell, C. A. McLennon, C. E. Schmidt, J. B. Shear, *Adv. Funct. Mater.* **2013**, *23*, 333.
- [34] A. Selimis, V. Mironov, M. Farsari, *Microelectron. Eng.* **2015**, *132*, 83.
- [35] W. Xiong, Y. S. Zhou, W. J. Hou, L. J. Jiang, Y. Gao, L. S. Fan, L. Jiang, J. F. Silvain, Y. F. Lu, *Sci. Rep.* **2014**, *4*, 4892.
- [36] D. Wu, J. Xu, L.-G. Niu, S.-Z. Wu, K. Midorikawa, K. Sugioka, *Light: Sci. Appl.* **2015**, *4*, e228.
- [37] J. C. Ng, L. Qian, P. R. Herman, *Opt. Lett.* **2016**, *41*, 1022.
- [38] K.-J. Lee, J. Hee An, C. W. Ha, Y. Son, D.-Y. Yang, J. Jung, K.-S. Lee, J.-W. Choi, *J. Biomed. Nanotechnol.* **2016**, *12*, 2125.
- [39] K. Sugioka, Y. Cheng, *Light: Sci. Appl.* **2014**, *3*, e149.
- [40] X. Wang, A. A. Kuchmizhak, E. Brasselet, S. Juodkazis, *Appl. Phys. Lett.* **2017**, *110*, 181101.
- [41] Y.-L. Zhang, Q.-D. Chen, H. Xia, H.-B. Sun, *Nano Today* **2010**, *5*, 435.
- [42] S. Kawata, H. B. Sun, T. Tanaka, K. Takada, *Nature* **2001**, *412*, 697.
- [43] W. Kaiser, C. G. B. Garrett, *Phys. Rev. Lett.* **1961**, *7*, 229.
- [44] Z. C. Ma, Q. D. Chen, B. Han, X. Q. Liu, J. F. Song, H. B. Sun, *Sci. Rep.* **2015**, *5*, 17712.
- [45] M. Malinauskas, M. Farsari, A. Piskarskas, S. Juodkazis, *Phys. Rep.* **2013**, *533*, 1.
- [46] K. Obata, A. El-Tamer, L. Koch, U. Hinze, B. N. Chichkov, *Light: Sci. Appl.* **2013**, *2*, e116.
- [47] T. Gissibl, S. Thiele, A. Herkommer, H. Giessen, *Nat. Photonics* **2016**, *10*, 554.
- [48] W. Xiong, Y. S. Zhou, X. N. He, Y. Gao, M. Mahjouri-Samani, L. Jiang, T. Baldacchini, Y. F. Lu, *Light: Sci. Appl.* **2012**, *1*, e6.
- [49] S. Rekštytė T. Jonavičius, D. Gailevičius, M. Malinauskas, V. Mizeikis, E. G. Gamaly, S. Juodkazis, *Adv. Opt. Mater.* **2016**, *4*, 1209.
- [50] C. N. LaFratta, J. T. Fourkas, T. Baldacchini, R. A. Farrer, *Angew. Chem., Int. Ed.* **2007**, *46*, 6238.
- [51] S. Maruo, J. T. Fourkas, *Laser Photonics Rev.* **2008**, *2*, 100.
- [52] L. Li, J. T. Fourkas, *Mater. Today* **2007**, *10*, 30.
- [53] Z. Lao, Y. Hu, C. Zhang, L. Yang, J. Li, J. Chu, D. Wu, *ACS Nano* **2015**, *9*, 12060.
- [54] J. Ni, C. Wang, C. Zhang, Y. Hu, L. Yang, Z. Lao, B. Xu, J. Li, D. Wu, J. Chu, *Light: Sci. Appl.* **2017**, *6*, e17011.
- [55] H. Zeng, D. Martella, P. Wasylczyk, G. Cerretti, J. C. Lavocat, C. H. Ho, C. Parmeggiani, D. S. Wiersma, *Adv. Mater.* **2014**, *26*, 2319.
- [56] Y.-L. Sun, W.-F. Dong, L.-G. Niu, T. Jiang, D.-X. Liu, L. Zhang, Y.-S. Wang, Q.-D. Chen, D.-P. Kim, H.-B. Sun, *Light: Sci. Appl.* **2014**, *3*, e129.
- [57] M. Malinauskas, A. Žukauskas, S. Hasegawa, Y. Hayasaki, V. Mizeikis, R. Buividas, S. Juodkazis, *Light: Sci. Appl.* **2016**, *5*, e16133.
- [58] F. Stellacci, C. A. Bauer, T. Meyer-Friedrichsen, W. Wenseleers, V. Alain, S. M. Kuebler, S. J. K. Pond, Y. D. Zhang, S. R. Marder, J. W. Perry, *Adv. Mater.* **2002**, *14*, 194.
- [59] A. Ishikawa, T. Tanaka, S. Kawata, *Appl. Phys. Lett.* **2006**, *89*, 113102.
- [60] B. B. Xu, H. Xia, L. G. Niu, Y. L. Zhang, K. Sun, Q. D. Chen, Y. Xu, Z. Q. Lv, Z. H. Li, H. Misawa, H. B. Sun, *Small* **2010**, *6*, 1762.

- [61] W. E. Lu, M. L. Zheng, W. Q. Chen, Z. S. Zhao, X. M. Duan, *Phys. Chem. Chem. Phys.* **2012**, *14*, 11930.
- [62] E. Blasco, J. Muller, P. Muller, V. Trouillet, M. Schon, T. Scherer, C. Barner-Kowollik, M. Wegener, *Adv. Mater.* **2016**, *28*, 3592.
- [63] S. Shukla, X. Vidal, E. P. Furlani, M. T. Swihart, K.-T. Kim, Y.-K. Yoon, A. Urbas, P. N. Prasad, *ACS Nano* **2011**, *5*, 1947.
- [64] S. Shukla, E. P. Furlani, X. Vidal, M. T. Swihart, P. N. Prasad, *Adv. Mater.* **2010**, *22*, 3695.
- [65] T. Tanaka, A. Ishikawa, S. Kawata, *Appl. Phys. Lett.* **2006**, *88*, 081107.
- [66] Y.-Y. Cao, X.-Z. Dong, N. Takeyasu, T. Tanaka, Z.-S. Zhao, X.-M. Duan, S. Kawata, *Appl. Phys. A: Mater. Sci. Process.* **2009**, *96*, 453.
- [67] Y. Y. Cao, N. Takeyasu, T. Tanaka, X. M. Duan, S. Kawata, *Small* **2009**, *5*, 1144.
- [68] W.-E. Lu, Y.-L. Zhang, M.-L. Zheng, Y.-P. Jia, J. Liu, X.-Z. Dong, Z.-S. Zhao, C.-B. Li, Y. Xia, T.-C. Ye, X.-M. Duan, *Opt. Mater. Express* **2013**, *3*, 1660.
- [69] S. Ren, Q. Wang, Y. Wang, S. Qu, *J. Phys. D: Appl. Phys.* **2012**, *45*, 285303.
- [70] P. W. Wu, W. Cheng, I. B. Martini, B. Dunn, B. J. Schwartz, E. Yablonovitch, *Adv. Mater.* **2000**, *12*, 1438.
- [71] K. Kaneko, H.-B. Sun, X.-M. Duan, S. Kawata, *Appl. Phys. Lett.* **2003**, *83*, 1426.
- [72] T. Baldacchini, A. C. Pons, J. Pons, C. N. LaFratta, J. T. Fourkas, Y. Sun, M. J. Naughton, *Opt. Express* **2005**, *13*, 1275.
- [73] C. N. LaFratta, D. Lim, K. O'Malley, T. Baldacchini, J. T. Fourkas, *Chem. Mater.* **2006**, *18*, 2038.
- [74] S. Maruo, T. Saeki, *Opt. Express* **2008**, *16*, 1174.
- [75] L. Vurth, P. Baldeck, O. Stéphan, G. Vitrant, *Appl. Phys. Lett.* **2008**, *92*, 171103.
- [76] R. Ameloot, M. B. Roeflaers, G. De Cremer, F. Vermoortele, J. Hofkens, B. F. Sels, D. E. De Vos, *Adv. Mater.* **2011**, *23*, 1788.
- [77] K. Vora, S. Kang, S. Shukla, E. Mazur, *Appl. Phys. Lett.* **2012**, *100*, 063120.
- [78] S. Kang, K. Vora, E. Mazur, *Nanotechnology* **2015**, *26*, 121001.
- [79] M. Terakawa, M. L. Torres-Mapa, A. Takami, D. Heinemann, N. N. Nedyalkov, Y. Nakajima, A. Hordt, T. Ripken, A. Heisterkamp, *Opt. Lett.* **2016**, *41*, 1392.
- [80] V. Mizeikis, S. Juodkazis, R. Tarozaite, J. Juodkazyte, K. Juodkazis, H. Misawa, *Opt. Express* **2007**, *15*, 8454.
- [81] K. Kaneko, K. Yamamoto, S. Kawata, H. Xia, J.-F. Song, H.-B. Sun, *Opt. Lett.* **2008**, *33*, 1999.
- [82] R. Malureanu, A. Alabastri, W. Cheng, R. Kiyani, B. Chichkov, A. Andryeuskii, A. Lavrinenko, *Appl. Phys. A: Mater. Sci. Process.* **2010**, *103*, 749.
- [83] J. Li, M. D. M. Hossain, B. Jia, D. Buso, M. Gu, *Opt. Express* **2010**, *18*, 4491.
- [84] A. Radke, T. Gissibl, T. Klotzbucher, P. V. Braun, H. Giessen, *Adv. Mater.* **2011**, *23*, 3018.
- [85] W.-K. Wang, Z.-B. Sun, M.-L. Zheng, X.-Z. Dong, Z.-S. Zhao, X.-M. Duan, *J. Phys. Chem. C* **2011**, *115*, 11275.
- [86] T. Ikegami, M. P. Stocker, K. Monaco, J. T. Fourkas, S. Maruo, *Jpn. J. Appl. Phys.* **2012**, *51*, 06FL17.
- [87] L. Ren, D. G. Wang, L. G. Niu, B. B. Xu, J. F. Song, Q. D. Chen, H. B. Sun, *Phys. Chem. Chem. Phys.* **2013**, *15*, 9590.
- [88] A. Tal, Y.-S. Chen, H. E. Williams, R. C. Rumpf, S. M. Kuebler, *Opt. Express* **2007**, *15*, 18283.
- [89] P. Jiang, J. Cizeron, J. F. Bertone, V. L. Colvin, *J. Am. Chem. Soc.* **1999**, *121*, 7957.
- [90] K. M. Kulinowski, P. Jiang, H. Vaswani, V. L. Colvin, *Adv. Mater.* **2000**, *12*, 833.
- [91] P. Nagpal, S. E. Han, A. Stein, D. J. Norris, *Nano Lett.* **2008**, *8*, 3238.
- [92] T. A. Walsh, J. A. Bur, Y.-S. Kim, T.-M. Lu, S.-Y. Lin, *J. Opt. Soc. Am. B* **2009**, *26*, 1450.
- [93] S. Tottori, L. Zhang, F. Qiu, K. K. Krawczyk, A. Franco-Obregon, B. J. Nelson, *Adv. Mater.* **2012**, *24*, 811.
- [94] S. Tottori, L. Zhang, K. E. Peyer, B. J. Nelson, *Nano Lett.* **2013**, *13*, 4263.
- [95] S. Kim, F. Qiu, S. Kim, A. Ghanbari, C. Moon, L. Zhang, B. J. Nelson, H. Choi, *Adv. Mater.* **2013**, *25*, 5863.
- [96] A. Barbot, D. Decanini, G. Hwang, *Sci. Rep.* **2016**, *6*, 19041.
- [97] X. Xiong, Z.-H. Xue, C. Meng, S.-C. Jiang, Y.-H. Hu, R.-W. Peng, M. Wang, *Phys. Rev. B* **2013**, *88*, 115105.
- [98] L. C. Montemayor, L. R. Meza, J. R. Greer, *Adv. Eng. Mater.* **2014**, *16*, 184.
- [99] L. C. Montemayor, J. R. Greer, *J. Appl. Mech.* **2015**, *82*, 071012.
- [100] R. Liontas, J. R. Greer, *Acta Mater.* **2017**, *133*, 393.
- [101] F. Formanek, N. Takeyasu, T. Tanaka, K. Chiyoda, A. Ishikawa, S. Kawata, *Appl. Phys. Lett.* **2006**, *88*, 083110.
- [102] F. Formanek, N. Takeyasu, T. Tanaka, K. Chiyoda, A. Ishikawa, S. Kawata, *Opt. Express* **2006**, *14*, 800.
- [103] Y. S. Chen, A. Tal, D. B. Torrance, S. M. Kuebler, *Adv. Funct. Mater.* **2006**, *16*, 1739.
- [104] Y.-S. Chen, A. Tal, S. M. Kuebler, *Chem. Mater.* **2007**, *19*, 3858.
- [105] S. M. Kuebler, A. Narayanan, D. E. Karas, K. M. Wilburn, *Macromol. Chem. Phys.* **2014**, *215*, 1533.
- [106] R. A. Farrer, C. N. LaFratta, L. J. Li, J. Praino, M. J. Naughton, B. E. A. Saleh, M. C. Teich, J. T. Fourkas, *J. Am. Chem. Soc.* **2006**, *128*, 1796.
- [107] K. Terzaki, N. Vasilantonakis, A. Gaidukeviciute, C. Reinhardt, C. Fotakis, M. Vamvakaki, M. Farsari, *Opt. Mater. Express* **2011**, *1*, 586.
- [108] N. Vasilantonakis, K. Terzaki, I. Sakellari, V. Puryls, D. Gray, C. M. Soukoulis, M. Vamvakaki, M. Kafesaki, M. Farsari, *Adv. Mater.* **2012**, *24*, 1101.
- [109] J. K. Gansel, M. Thiel, M. S. Rill, M. Decker, K. Bade, V. Saile, G. von Freymann, S. Linden, M. Wegener, *Science* **2009**, *325*, 1513.
- [110] J. K. Gansel, M. Latzel, A. Frölich, J. Kaschke, M. Thiel, M. Wegener, *Appl. Phys. Lett.* **2012**, *100*, 101109.
- [111] J. Kaschke, M. Wegener, *Opt. Lett.* **2015**, *40*, 3986.
- [112] J. Kaschke, M. Blome, S. Burger, M. Wegener, *Opt. Express* **2014**, *22*, 19936.
- [113] J. Kaschke, J. K. Gansel, M. Wegener, *Opt. Express* **2012**, *20*, 26012.
- [114] X. W. Gu, J. R. Greer, *Extreme Mech. Lett.* **2015**, *2*, 7.
- [115] M. M. Hossain, M. Gu, *Opt. Mater. Express* **2012**, *2*, 996.
- [116] O. M. Marago, P. H. Jones, P. G. Gucciardi, G. Volpe, A. C. Ferrari, *Nat. Nanotechnol.* **2013**, *8*, 807.
- [117] M. Daly, M. Sergides, S. Nic Chormaic, *Laser Photonics Rev.* **2015**, *9*, 309.
- [118] M. Gu, H. Bao, X. Gan, N. Stokes, J. Wu, *Light: Sci. Appl.* **2014**, *3*, e126.
- [119] A. Lehmuskero, P. Johansson, H. Rubinsztein-Dunlop, L. Tong, M. Kall, *ACS Nano* **2015**, *9*, 3453.
- [120] A. Ashkin, J. M. Dziedzic, J. E. Bjorkholm, S. Chu, *Opt. Lett.* **1986**, *11*, 288.
- [121] K. Dholakia, P. Reece, *Nano Today* **2006**, *1*, 18.
- [122] D. G. Grier, *Nature* **2003**, *424*, 810.
- [123] H. Wang, S. Liu, Y. L. Zhang, J. N. Wang, L. Wang, H. Xia, Q. D. Chen, H. Ding, H. B. Sun, *Sci. Technol. Adv. Mater.* **2015**, *16*, 024805.
- [124] B. B. Xu, R. Zhang, H. Wang, X. Q. Liu, L. Wang, Z. C. Ma, Q. D. Chen, X. Z. Xiao, B. Han, H. B. Sun, *Nanoscale* **2012**, *4*, 6955.
- [125] P. Buffat, J. P. Borel, *Phys. Rev. A* **1976**, *13*, 2287.
- [126] I. Shyjumon, M. Gopinadhan, O. Ivanova, M. Quaas, H. Wulff, C. A. Helm, R. Hippler, *Eur. Phys. J. D* **2005**, *37*, 409.
- [127] Y. Son, J. Yeo, H. Moon, T. W. Lim, S. Hong, K. H. Nam, S. Yoo, C. P. Grigoropoulos, D. Y. Yang, S. H. Ko, *Adv. Mater.* **2011**, *23*, 3176.
- [128] C. W. Cheng, J. K. Chen, *Appl. Phys. A: Mater. Sci. Process.* **2016**, *122*, 289.
- [129] B. B. Xu, D. D. Zhang, X. Q. Liu, L. Wang, W. W. Xu, M. Haraguchi, A. W. Li, *Opt. Lett.* **2014**, *39*, 434.

- [130] A. Ishikawa, T. Tanaka, *IEEE J. Sel. Top. Quantum Electron.* **2013**, *19*, 4700110.
- [131] S. Bordács, I. Kézsmárki, D. Szaller, L. Demkó, N. Kida, H. Murakawa, Y. Onose, R. Shimano, T. Rößm, U. Nagel, S. Miyahara, N. Furukawa, Y. Tokura, *Nat. Phys.* **2012**, *8*, 734.
- [132] M. Decker, M. W. Klein, M. Wegener, S. Linden, *Opt. Lett.* **2007**, *32*, 856.
- [133] J. B. Pendry, *Science* **2004**, *306*, 1353.
- [134] N. J. Halas, S. Lal, W. S. Chang, S. Link, P. Nordlander, *Chem. Rev.* **2011**, *111*, 3913.
- [135] B. B. Xu, Z. C. Ma, L. Wang, R. Zhang, L. G. Niu, Z. Yang, Y. L. Zhang, W. H. Zheng, B. Zhao, Y. Xu, Q. D. Chen, H. Xia, H. B. Sun, *Lab Chip* **2011**, *11*, 3347.
- [136] I. Izquierdo-Lorenzo, S. Jradi, P.-M. Adam, *RSC Adv.* **2014**, *4*, 4128.
- [137] B.-B. Xu, L. Wang, Z.-C. Ma, R. Zhang, Q.-D. Chen, C. Lv, B. Han, X.-Z. Xiao, X.-L. Zhang, Y.-L. Zhang, K. Ueno, H. Misawa, H.-B. Sun, *ACS Nano* **2014**, *8*, 6682.
- [138] D. Naumenko, L. Stolzer, A. S. Quick, D. Abt, M. Wegener, C. Barner-Kowollik, S. D. Zilio, B. Marmiroli, H. Amenitsch, L. Fruk, M. Lazzarino, *J. Mater. Chem. C* **2016**, *4*, 6152.
- [139] Z.-C. Ma, Y.-L. Zhang, B. Han, X.-Q. Liu, H.-Z. Zhang, Q.-D. Chen, H.-B. Sun, *Adv. Mater. Technol.* **2017**, *2*, 1600270.
- [140] K. Sun, Z. Wang, X. Jiang, *Lab Chip* **2008**, *8*, 1536.
- [141] B. B. Xu, Y. L. Zhang, H. Xia, W. F. Dong, H. Ding, H. B. Sun, *Lab Chip* **2013**, *13*, 1677.